Spring 2015

Numerical simulation and characterization of jet flows in indoor environments

Zhu Shi
Purdue University

Graduate School Form 30
Updated 1/15/2015

PURDUE UNIVERSITY
GRADUATE SCHOOL
Thesis/Dissertation Acceptance

This is to certify that the thesis/dissertation prepared

By Zhu Shi

Entitled

NUMERICAL SIMULATION AND CHARACTERIZATION OF JET FLOWS IN INDOOR ENVIRONMENTS

For the degree of Master of Science in Mechanical Engineering

Is approved by the final examining committee:

Qingyan Chen
Co-chair

Jun Chen
Co-chair

Chao-Hsin Lin

To the best of my knowledge and as understood by the student in the Thesis/Dissertation Agreement, Publication Delay, and Certification Disclaimer (Graduate School Form 32), this thesis/dissertation adheres to the provisions of Purdue University's "Policy of Integrity in Research" and the use of copyright material.

Approved by Major Professor(s): Qingyan Chen

Approved by: Ganesh Subbarayan 3/4/3015

Head of the Departmental Graduate Program Date

NUMERICAL SIMULATION AND CHARACTERIZATION OF JET FLOWS IN INDOOR ENVIRONMENTS

A Thesis

Submitted to the Faculty

of

Purdue University

by

Zhu Shi

In Partial Fulfillment of the

Requirements for the Degree

of

Master of Science in Mechanical Engineering

May 2015

Purdue University

West Lafayette, Indiana

For my parents.

ACKNOWLEDGEMENTS

First of all, I would like to express my sincere appreciation to my advisors Prof. Qingyan(Yan) Chen and Prof. Jun Chen, for their continuous support and guidance. Their immersed knowledge, rich experience and rigorous academic attitude are what led me step by step in my study, research, and scientific writing. I also learnt a lot from their enthusiasm towards the unknown world, and the ways they balance work and life. I could not imagine completing the thesis without their help and patience. My special thanks also go to Dr. Chao-Hsin Lin, a technical fellow from Boeing Inc., for serving as my committee member, and his time devoted to my defense and thesis.

I would like to thank my lab mates, Mr. Mingang Jin, Aakash Rai, Chun Chen, Wei Liu, Haojie Wang, Dayi Lai, Duo Xu, Jian Gao, Nicolas Pohl, Zijie Qu, Xiangyu Gao, Ranchi Chen as well as Ms. Anna Kerlo, Nina Zhou, Yan Xue, and Ruoyu You for their advice in my research and their help in my life. Discussions with them gave me a lot of inspiration for my thesis. The experience of studying and working together with them will never fade in my memory. I also appreciate the help of Mr. Frank Lee, Mr. Ron Evans and Mr. Bob Brown from Herrick shop in my research work.

Finally, I want to express great gratitude to my parents for their unconditional love and support throughout my life. I am also very thankful to my girlfriend, Xinyun, for always understanding and standing by me in the good times and bad.

TABLE OF CONTENTS

Page

Page

LIST OF TABLES

LIST OF FIGURES

Figure Page

NOMENCLATURE

C_j	Concentration of species j
D	Diameter of jet nozzle, characteristic length scale
D_t	Turbulent eddy diffusivity
g_i	Gravitational acceleration in i direction
G_b	The generation of turbulence kinetic energy due to buoyancy
G_k	The generation of turbulence kinetic energy due to the mean velocity gradients
I	Turbulent intensity
p	Pressure
P_{jk}	Stress production
Re	Reynolds number
Ri	Richardson number
$r_{-1/2}$, $r_{+1/2}$, $x_{1/2}$	The half-width of jet
S_ϕ	Source term of scalar ϕ
Sc_t, $\sigma_{C,t}$	Turbulent Schmidt number
t	Time
U	Mean velocity
u_i	Velocity magnitude in i direction
U_0	Jet initial velocity, characteristic velocity
x_i	Coordinate in i direction

Y_k	Dissipation of k due to turbulence
Y_ω	Dissipation of ω due to turbulence
Z_{peak}	Z coordinate of peak velocity location on jet axis
ρ	Density
ϕ	Scalar component
k	Kinetic energy per unit mass
ε	Turbulent dissipation rate
ω	Specification dissipation rate
$\Gamma_{\phi,eff}$	Coefficient of effective diffusion of scalar ϕ
μ	Dynamic viscosity
μ_t	Turbulent dynamic viscosity
σ_C	Schmidt number
τ_{ij}	Shear stress
Δ	Change in variable
θ	Non-dimensional density difference
ν_t	Turbulent kinematic viscosity
δ	Normalized z location along jet axis
Ω_i	Vorticity in i direction
χ	Normalized x location
η	Fresh air ratio

ABSTRACT

Shi, Zhu. M.S.M.E., Purdue University, May 2015. Numerical Simulation and Characterization of Jet Flows in Indoor Environments. Major Professors: Qingyan Chen and Jun Chen, School of Mechanical Engineering.

Jet flows are prevalent in indoor environment and other engineering applications. Typical examples in indoor environment include the flow discharged from personal ventilation systems, and the jet exhaled through breathing or coughing. When there is density (or temperature) difference between the jet and surroundings, jet flow becomes stratified jet. Due to its complication, stratified jet flow is difficult to model, especially in the developing or transitional region of the flow. Studying stratified jet flows is of great significance for understanding the mixing dynamics of jet and ambient environment. This is particularly important for optimizing indoor environment design, or obtaining accurate boundary conditions in indoor air flow simulations.

Various turbulence models have been used to simulate stratified flows. This investigation systematically evaluated the performance of seven turbulence models under different turbulence levels and stratification levels, by comparing simulation results with experimental data. Mean velocity, turbulent kinetic energy and turbulent shear stress were examined in the comparisons. Mean square error values were used to quantify the evaluation. For the weakly stratified jet, all seven models could predict well the mean velocity, but for the strongly stratified jet, the Reynolds stress model and LES

overpredicted the velocity in the unstable stratification region. SST $k-\omega$ was the overall best model. This investigation also analyzed the computing costs of the models as well as the vorticity and entrainment ratios predicted in the simulation.

This study introduced a new dynamic turbulent Schmidt number model which can determine turbulent Schmidt number based on local flow structure. The proposed model can improve the prediction of density distribution especially at downstream locations, although it takes 10% additional computing time.

Furthermore, this study developed a CFD model to investigate gasper-induced jet flow. The results indicated that the jet centerline velocity profile could collapse into a universal curve after normalization; meanwhile, the lateral velocity profiles at downstream locations followed self-similarity rule. Based on that, the study proposed two models to predict normalized velocity at jet centerline, and lateral velocity at downstream locations, respectively. A flow rate model was also developed to predict the mainstream flow rates at various downstream locations of gasper-induced jet. The CFD model and developed flow rate model were further used to assess the impact of gasper on air quality in the breathing zones of passengers.

CHAPTER 1. INTRODUCTION

1.1 Background and Significance

With the development of aviation technology, travelling by air has become increasingly popular among passengers. According to International Air Transport Association (IATA) (2013), 2.98 billion passengers took airplanes in the year 2012; and by 2017, the estimated air traffic passenger number will be 3.91 billion. The duration of a regular flight ranges from 1 to 2 hours, to more than 12 hours for international flights. The high occupant density, limited air flow rate, and sometimes long flight durations make the aircraft cabin of high risk of airborne disease transmission. In 1993, an investigation demonstrated the transmission of one flight attendant's infectious tuberculosis (TB) to other flight crew members (Kenyon et al. 1996). Another case for such passenger-to-passenger transmissions was the severe acute respiratory syndrome (SARS), which caused more than 700 deaths worldwide, and spread partially due to flight travels of persons infected with SARS (Olsen et al. 2003). The possibility of passengers to get infected with airborne diseases through respiration makes it fairly important to study the air flow inside aircraft cabin as well as other indoor environments.

Besides indoor air quality, thermal comfort is another important factor for passengers' experience during the flight travel. It was reported that passengers in long duration flight

with thermal discomfort may experience symptoms such as tiredness, headache (Zhang et al. 2010), and even showed symptoms similar to acute mountain sickness, like nausea, vomiting or sleep disturbance (Air Transport medicine Committee 1997; Brown et al. 2001; Muhm et al. 2007). Thermal comfort in aircraft cabin is mainly determined by the air velocity and air temperature distributions (Kühn et al. 2009), although other parameters like humidity (Zhang et al. 2010) can influence it as well. Studying airflow inside aircraft cabin plays an important role in improving thermal comfort of passengers by providing guidance for the design and development of cabin and its ventilation systems (Kühn et al. 2009).

Air distribution in aircraft cabin is mainly controlled by ECS (Environmental Control System), which regulates the temperature, pressure and contaminant level inside cabin (Wu and Ahmed 2011). Currently mixing air distribution system is used in many aircraft cabins. In this system, fresh air is supplied from the ceiling, and after it is mixed with the existing air inside cabin, air is exhausted from the ground level. Due to complicated cabin design, however, detailed airflow distribution is determined by a lot of factors including cabin geometry, seat positions, and air supply locations (Zhang et al. 2010). Moreover, there are other types of flows inside cabin which interplay with the flow induced by main ventilation system. Jet flow is a common one among these types of flows. For example, gasper, which is installed above every passenger's seat, introduces a typical jet flow when it is switched on. Another example is the air exhaled by people's mouth or nose (Gupta et al. 2010) (Figure 1.1). These abovementioned jet flows, although usually with low flow rate, could still have large impact on local air flow distribution and air quality.

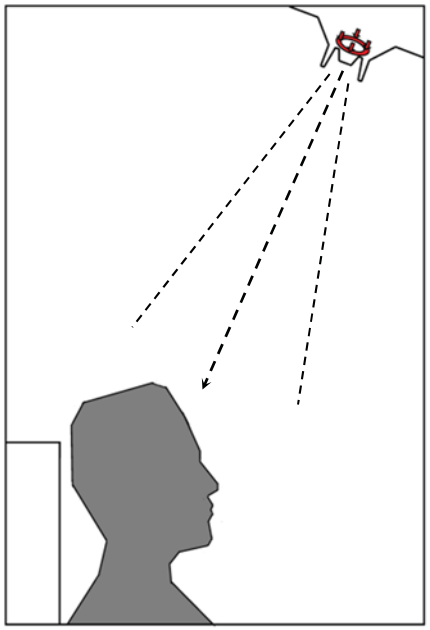

(a) Gasper-induced jet flow

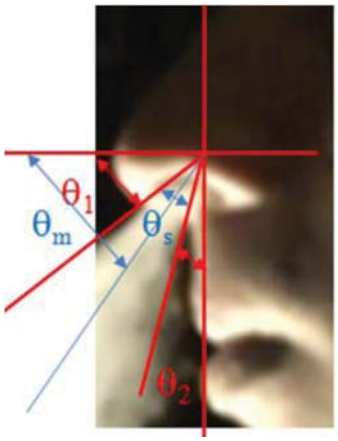

(b) Nose breathing (Gupta et al. 2010)

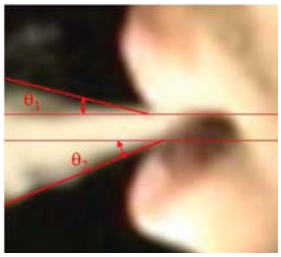

(c) Mouth breathing (Gupta et al. 2010)

Figure 1.1. Jet flows in aircraft cabin

Jet flows are not only common in aircraft cabin, but also prevalently seen in other indoor environments. Depending on the surrounding environments, indoor jet can develop into free jet (Melikov 2004), plane jet (Van Hooff et al. 2012), impinging jet (Karimipanah and Awbi 2002), or wall jet (Davidson et al. 2003), after discharged from jet nozzle. Most jets existing in indoor environment are turbulent jets, which makes it complex in physics, especially in the transitional or developing regions. Understanding the flow characteristics of jet flows in indoor environment is of significant importance for comprehending not only how the abovementioned jets develop in offices or enclosed vehicles, but also how they can influence indoor air quality and thermal comfort for human beings. On the other hand, good characterization of jet flow development can

provide accurate guidance for setting boundary conditions of indoor jets in indoor air flow simulation, when it is needed to define boundary conditions at a jet downstream, instead of the jet nozzle neck.

Many times the indoor jet discharged from jet nozzle has a slightly different density with ambient air (due to their different temperatures), which makes the jet flow stratified. Due to its prevalence in nature and complexity in physics, stratified flows have been investigated in a lot of researches. Various experimental investigations have been carried out to explore the characteristics of stratified flows. The measurement techniques included using traditional instruments such as hot-wire anemometers (Hunt and Snyder 1980; Lienhard and Van Atta 1990), sonic/ultrasonic anemometers (Mahrt et al. 2001), laser Doppler anemometers (Kneller et al 1999; Komori et al. 1983), and more advanced technologies like particle image velocimetry (PIV) (Dalziel et al. 2007) and planar laser-induced fluorescence (PLIF) (Xu and Chen 2012). These experiments probed the physics behind stratified flows, and more importantly, provided valuable dataset for model developing in such problems. With the development of computational resources, computational fluid dynamics (CFD) has become increasingly popular in investigating the stratified flow problem. Direct numerical simulation (DNS) is one of the CFD simulation methods. It resolves the whole spectrum of all turbulent scales and requires no modeling (ANSYS 2011). Jacobitz et al. (1997) performed DNS to study the evolution of turbulence in a uniformly sheared and stably stratified flow. Despite its good accuracy in flow prediction, however, DNS simulation is not practical in most engineering cases due to its high cost in computational resources. Reynolds-averaged Navier-Stokes (RANS)

and large eddy simulation (LES) are more widely used in engineering problems. RANS equations modeled the whole range of scales of turbulence, and govern the transport of averaged flow quantities. In this way, the computation effort was reduced to a large degree. In RANS simulation of stratified flows, most researches utilized two-equation models, such as standard $k-\varepsilon$, realizable $k-\varepsilon$ and renormalization group (RNG) $k-\varepsilon$ (Liu et al. 2008; Spall 1998; Umlauf et al. 2003), standard $k-\omega$, and shear stress transport (SST) $k-\omega$ (Ji et al. 2008; Cropper et al. 2010), or seven-equation models, such as Reynolds stress model (RSM) (Peeters et al. 1992). As for LES, it computes large eddies explicitly in a time-dependent simulation using "filtered" Navier-Stokes equations, but small eddies are still modeled. Thus in terms of fraction of resolved scales and computational cost, LES falls between DNS and RANS. Su et al. (1998) used LES to investigate the turbulent channel flow under a wide range of stable stratification levels, and found that increase of stable stratification leaded to remarkable changes in the characteristics of wall-bounded turbulence. Nevertheless, despite the many CFD studies focused on stratified flows using RANS and LES, there has still been no systematic evaluation of the performance of different turbulent models at different turbulence and stratification levels, indicated by Reynolds numbers (Re) and Richardson numbers (Ri), respectively. This is particularly important in the transitional or developing region of the flow since most of the previous studies have been focused on fully developed regions where many turbulence models have been proven to function well in unstratified flows.

Furthermore, in the simulations of stratified flows, a key parameter in predicting density distribution is the turbulent Schmidt number (Sc_t) (Schumann and Gerz 1995). It is

defined as the ratio of the turbulent momentum diffusivity (eddy viscosity) and the turbulent mass diffusivity, and thus has a large impact on the spreading rate of one species to another. In most current researches, constant turbulent Schmidt number was assumed in CFD simulations, which was not always reasonable (He et al. 1999; Tominaga and Stathopoulos 2007). He et al. (1999) identified the significant effect of the turbulent Schmidt number on the species spreading rate in a jet-in-cross flows. The authors also concluded that Sc_t should be a variable in jet-in-cross flows based on a semi-empirical analysis. Tominaga and Stathopoulos (2007) discovered that the optimal turbulent Schmidt number depended on local flow characteristics and recommended a dynamic determination of Sc_t according to local flow structure. Since Sc_t has a large impact on the species transfer in simulating stratified flows, adopting such a dynamic model is more reasonable than using a constant turbulent Schmidt number in simulating stratified flows.

The studies on turbulence models and turbulent Schmidt number provide fundamentals for simulating the real jet flow problems in indoor environment, like gasper-induced jet flow. As a common personalized ventilation system in vehicles such as bus and aircrafts, gasper is installed to customize thermal comfort by adjusting the angle and opening of gasper for each passenger to change the discharged jet flow rate. A typical gasper is composed of an adjustable annular air outlet and a cone within it, which makes the jet flow complicated. Characterizing the gasper-induced jet flows is of significance for understanding how airflow interplays with the ambient after it is discharged from gasper outlet. Therefore, it is important to understand the air decontaminating effect of the

gasper. Previous study (Gupta et al. 2011) used a circular outlet to represent a gasper outlet in simulating gasper-induced flows. This simplified geometry saved computational efforts significantly, but at the same time led to inaccuracy of flow prediction, particularly in locations close to gasper outlet. Most of other experimental and computational researches that investigated fresh air rate, e.g., Ricou and Spalding (1961) and Olsson and Fuchs (1996), were also focused on simple round jets. Thus there is a need to incorporate the realistic gasper geometry in studying the flow characteristics of gasper-induced jets and evaluating gasper's air decontaminating effect in a passenger's breathing zone.

1.2 Objectives and Roadmap

There are three major objectives in this current research: (1) to systematically evaluate the performances of most prevalent turbulence models in simulating stratified jets, under different turbulence levels and stratification levels; (2) to further investigate the impact of the turbulent Schmidt number in simulating stratified jets, and to develop a dynamic Schmidt number model based on local flow structure; (3) to investigate the flow characteristics of gasper-induced jet flow by incorporating its realistic nozzle geometry and to assess its effect on air quality in passenger's breathing zone.

This investigation conducted the following four tasks in order to achieve the abovementioned objectives:

Task 1: Literature Review

The study first did literature review on current research status in six aspects. The first aspect is the previous researches on air distribution inside aircraft cabin. The second one is numerical studies that have been done on indoor jet flows. The third aspect is the numerical studies on stratified flows. The fourth one is literature on quantitative evaluation of the deviation degree of two sets of data. The fifth aspect is the researches on the effect of turbulent Schmidt number in stratified flow simulation, and the importance of a variant turbulent Schmidt number model. The last part illustrates the experimental and numerical researches on gasper-induced flows.

Task 2: Numerical simulations of stratified jets and model performance evaluations

Numerical simulation of stratified jet flows under different turbulence levels and stratification levels was done. The experiment of Xu and Chen (2012) were used as benchmark to validate the simulation, and to evaluate the performances of 6 RANS models and one LES model in simulating stratified jets. Both 1^{st} order flow features (mean velocities) and 2^{nd} order flow characteristics (turbulent kinetic energy and shear stress) were taken into consideration in appraising model performances. The statistical parameter, mean square error (MSE) was adopted to quantitatively evaluate the deviation of simulated data from experimental results.

Task 3: Development for dynamic turbulent Schmidt number model

A new dynamic turbulent Schmidt number model was proposed based on local velocity gradient and density gradient. Experimental data from Xu and Chen (2012) was used for

model developing. The developed model can be used to replace the constant turbulent Schmidt number in stratified flow simulation, and can yield good predictions of scalar distributions.

Task 4: Simulation of gasper-induced jet flows and assessment of its air quality improvement

A CFD model that included detailed gasper geometry was built to study the flow pattern of gasper-induced jet flows. The simulation results were compared with experimental results for model validation. The simulation results were further used to discuss how the geometrical parameters and initial velocities affect the flow characteristics. Two mathematical models were developed to predict the centerline velocity profile, and lateral velocity profile in jet flows induced by gasper or nozzle with similar geometry. Based on these two models, another model for estimating the flow rates at various jet downstream locations was proposed. Furthermore, the effect of air quality improvement by gaspers was also evaluated using both CFD results and the developed flow rate model.

1.3 Outline of this Report

Chapter 2 reports the literature review of current research. Chapter 3 illustrates the numerical simulation of stratified flows and turbulence model performance of six RANS models and one LES model. Chapter 4 focuses on the model development of dynamic turbulent Schmidt number model. Chapter 5 presents gasper-induced jet flow simulation and the air quality improvement effect of such flow in indoor environment. Chapter 6

concludes this investigation, and proposes the future potential researches following this study.

CHAPTER 2. LITERATURE REVIEW

2.1 Air Distribution inside Aircraft Cabin

Over the past several decades, numerous investigations have been conducted to study the airflow inside aircraft cabin. Most of the investigations adopted the methods of experimental measurements or numerical simulations. For the experiments, most commonly used measurement tools included hotwire anemometers (Zhou et al. 2006) (Figure 2.1), hot sphere anemometers (Zhang et al. 2009) (Figure 2.2), particle streak velocimetry (PSV) (Zhang, Y. et al. 2005), particle tracking velocimetry (PTV) (Müller et al. 1997), particle image velocimetry (PIV) and so on (Liu et al. 2012a). For example, Zhou et al. (2006) used hotwire anemometer to measure fluctuation characteristics in dynamic airflows generated by a dynamic air supply terminal. Zhang et al. (2009) adopted 16 omni-directional hot-sphere anemometers to measure air velocity and temperature near the diffuser in an airliner cabin mockup. Lin et al. (2006) conducted PIV measurement to obtain airflow information in a generic cabin model. Many measurements considered the influence of passengers on airflow inside aircraft cabin, and different methods were used to represent passengers, including using heated cylinders (Sze To et al. 2009), box manikins (Zhang, Y. et al. 2005), thermal manikins (Wang et al. 2008), etc. These experimental measurements provided reliable results in terms of air velocity, but at the same time, can be time consuming and costly.

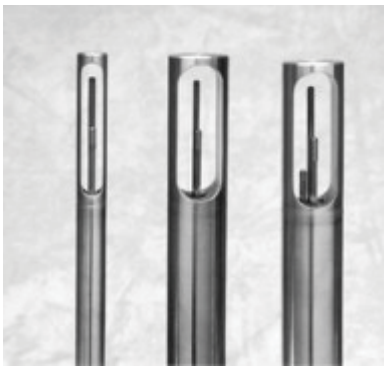

Figure 2.1. Hot wire anemometers (Liu et al. 2012a)

Figure 2.2. Hot sphere anemometers (Liu et al. 2012b)

On the other hand, the development of computational tools made it increasingly prevalent to use numerical simulation to investigate the airflow inside aircraft cabin. Most of the numerical studies used CFD method to calculate airflow velocity, temperature, humidity, and contaminant concentration (Liu et al. 2012a). And in the CFD models, standard $k-\varepsilon$ and RNG $k-\varepsilon$ are two most well-known turbulence models in simulating among RANS models in modeling such flow problems (Liu et al. 2012a; Yan et al. 2008; Mazumdar and Chen 2008). There were also studies (Lin et al. 2006) adopting LES to calculate airflow distribution in an aircraft cabin. These CFD models, once validated using experimental results, could be used for further analysis on airflow distribution in aircraft cabin.

In terms of the domains for experimental or numerical studies, many studies built cabin mockups for experimental data collection, and used corresponding computational domains for CFD simulation (Zhang and Chen 2007; Sze To et al. 2009). There were also studies carried out in functional commercial airliner (Liu et al. 2012b; Liu et al. 2013), which could give more reliable results and conclusions on airflow distributions.

2.2 Numerical Studies of Jet Flows in Indoor Environment

In indoor environment area, lots of numerical models were built, and validated using experimental data, after which these validated models were used to investigate different types of indoor jet problems. Davidson et al. (2003) used low-Re $k-\varepsilon$ model and v^2-f model to compute the flow in a three dimensional wall jet. Based on the results, they proposed two modifications for v^2-f model to improve 3D wall jet flow predictions. Karimipanah and Awbi (2002) carried out experiments on a new impinging jet ventilation system and compared its performance with a wall ventilation system. They also used experimental and numerical results to obtain air quality parameters such as ventilation efficiency and local mean age of air in a mock-up classroom. Russo et al. (2009) developed a CFD model of a novel personal ventilation jet flow directing towards the breathing zone of a seated manikin using realizable $k-\varepsilon$ model, and showed that the air quality of the novel personal ventilation system was sensitive to nozzle intensity and flow rate. Van Hooff et al. (2012) conducted PIV measurements and numerical analysis of a free plane jet with Coanda effect, and showed the Coanda effect caused a free plane jet to a wall jet right at the jet inlet. Gupta et al. (2010) used experimental measurements to characterize exhaled jet flow during breathing and talking. They found that the exhaled flow rate over time can be represented as a sinusoidal function for breathing and a constant during normal talking. Gupta et al. (2012) further used these experimental data as boundary conditions for CFD study, and assessed the risk of airborne diseases infection in airliner cabin. These investigations in indoor jet flows demonstrated the flow

characteristics of flow distributions in indoor environment while various types of jets were in presence.

2.3 Numerical Investigations of Stratified Flows

The complex physics behind stratified flows makes such flows difficult to be accurately described with numerical simulation models. Previous numerical studies on stratified flows adopted various methods and models to try to capture the key flow characteristics in such flow problems. Jacobitz et al. (1997) adopted DNS to investigate the turbulence evolution in uniformly sheared and stably stratified flows. They discovered the evolution of turbulence was strongly dependent on at least three parameters-Richardson number, the initial value of Taylor microscale Reynolds number, and the initial value of shear number. More commonly used CFD methods in stratified flow numerical simulation are using RANS or LES in predictions. Liu et al. (2008) studied the performances of the RNG $k-\varepsilon$ model and standard $k-\varepsilon$ model in simulating single-sided natural ventilation driven by stratification effect, which is due to temperature difference. Their comparison with experimental data concluded that the RNG $k-\varepsilon$ model performed better than the standard $k-\varepsilon$ model in predicting such flow. Ji et al. (2008) adopted the $k-\omega$ model (Wilcox 1988) to investigate naturally ventilated double skin facades with Venetian blinds inside the facade cavity. The results demonstrated that Venetian blinds could enhance the buoyancy-driven natural ventilation of the facade cavity. Cropper et al. (2010) developed a CFD model to simulate the airflow and temperatures around human body using the SST $k-\omega$ model (Menter 1994). This model was further coupled with a thermal comfort model, which was able to predict human thermal comfort in various

environmental conditions. Venayagamoorthy et al. (2003) tested the performance of the standard $k-\varepsilon$ model in stably stratified flows, using data from direct numerical simulation. Their results showed that the buoyancy parameter Cε3 was a very sensitive parameter for stratified flows. Besides the two-equation models, Spall (1998) adopted the Reynolds stress model (RSM), a seven-equation model, to investigate the natural stratification phenomenon in cylindrical thermal storage tanks, showing that the RSM model can give a more accurate prediction of the thermocline thickness than the $k-\varepsilon$ model. Armenio and Sarkar (2002) used LES method to investigate the stably stratified turbulent channel flow in a wide range of levels, and calculated the eddy diffusivity coefficients for the subgrid momentum flux and buoyancy flux. These numerical simulations provided detailed information concerning stratified flows, which was complimentary to the experimental results.

2.4 Statistical Parameters for Evaluating Model Performance

In the evaluation of model performance by comparing the simulation results with experimental data, literature suggested conducting quantitative comparison by using statistical parameters, which can provided more direct criteria for evaluation (Britter and Schatzmann 2007). Table 3 listed the most commonly used statistical parameters for quantifying model performances. In previous studies, Pullen et al. (2005) assessed the spatial extent of modeled contaminant transport caused by airborne agent in some urban areas using several parameters including fractional bias (FB), root mean square error (RMSE), percentage of points within a factor of 2 (FAC2). Franke et al. (2008) used FAC2, FB, geometric mean (MG), geometric variance (VG) etc. to evaluate the

simulation results of contaminant dispersion with different wind different directions, through comparison with wind tunnel experiments. Marmur and Mamane (2003) adopted Pearson's correlation coefficient (R), normalized mean square error (NMSE), FB and fractional variance (FS) to compare the performances of several mobile-source and line-source models in simulating air quality. Willmott and Matsuura (2005) compared the advantages of mean square error (MSE) and RMSE in assessing average model performance, and concluded that MSE is a more natural measure of average error, and is more unambiguous.

Table 2.1. Several commonly used statistical parameters for model performance evaluation.

Parameter	Definition	Note
FAC2	$\frac{1}{n}\sum_{i=1}^{n} N_i$	$N_i = \begin{cases} 1 & for\ 0.5 \le P_i/O_i \le 2 \\ 1 & for\ O_i \le W\ and\ P_i \le W \\ 0 & else \end{cases}$
FB	$\frac{\overline{O} - \overline{P}}{0.5(\overline{O} + \overline{P})}$	$\overline{P}$ is averaged predicted value; $\overline{O}$ is averaged observed value.
MG	$\exp\left(\overline{\ln O} - \overline{\ln P}\right)$	$O = \max(W, O)$ $P = \max(W, P)$
MSE	$\overline{(O-P)^2}$	
NMSE	$\frac{\overline{(O-P)^2}}{\overline{O}\,\overline{P}}$	
VG	$\exp\left[\overline{\left(\ln O - \ln P\right)^2}\right]$	$O = \max(W, O)$ $P = \max(W, P)$

2.5 Turbulent Schmidt Number

A lot of previous literatures mentioned the importance of turbulent Schmidt number in stratified flow simulations. The selection of Sc_t value has been controversial, which triggers many discussions. For example, Rohr et al. (1988) measured this value to be 0.63 in saltwater. Tavoularis and Corrsin (1981) made measurements in homogeneous turbulence in a wind tunnel, and found the value to be between 1 and 1.2. More recently, He et al. (1999) assessed the adequacy of assuming constant Schmidt number in predicting scalar field in a jet-in-crossflow, and observed that turbulent Schmidt number has a large influence on species spreading rate in such flows, especially when momentum flux ratio is small. Yimmer et al. (2002) found Sc_t increased monotonically in radial direction in the fully developed region of a jet, which implied the unreasonableness of presuming constant turbulent Schmidt number. Tominaga and Stathopoulos (2007) reviewed previous studies related to the application of optimum values of Sc_t, and found Sc_t was widely distributed in the range of 0.2-1.3 in various studies. They also concluded that different Sc_t values can have significant impact on simulation results. With all the above-mentioned findings, it is interesting to develop variant turbulent Schmidt number models in stratified flow simulations.

2.6 Experimental and Numerical Studies on Gasper Induced Flow

Anderson (2012) carried out experiment in a wide-body, 11-row Boeing 767 aircraft mockup using carbon dioxide (CO_2) as the tracer gas, to investigate the effect of gaspers on contaminant transport in aircraft cabin. Three series of experiments were conducted,

which led to three separate sets of conclusions. The final conclusion from Anderson (2012) was the impact of gasper jet had on contaminant transmission was dependent on the location of tracer gas plume and sampling location. On numerical simulation side, Gupta et al. (2011) built a CFD model which contained 15 million elements, to investigate the effect of gasper on contaminant transport in an aircraft cabin mockup. Circular outlets were used to represent the gaspers, and RNG $k-\varepsilon$ model was selected for the study. Their study found that the risk reduction effect of gaspers was very minor compared with the cases when gaspers are not turned on.

2.7 Discussions

In the CFD simulation of stratified jet flows, although there was a lot of literature reporting the results of similar flow problems using different turbulence models, there still lacks a systematic evaluation of model performances under different turbulence and stratification levels, in a quantitative way. Besides, although the suggested statistical parameters for evaluating model performances included FAC2, FB, MG, MSE, NMSE and VG (Britter and Schatzmann 2007; Pullen et al. 2005; Franke et al. 2008; Marmur and Mamane 2003; Willmott and Matsuura 2005), most of these parameters were introduced to appraise the performance of one specific turbulence model. In the current research, the focus is on comparing the performances of various turbulence models by evaluating the mean velocity, turbulent kinetic energy, shear stresses distributions. Thus using MSE is enough for making such evaluation, and it is a very straightforward parameter for quantifying the degree of the deviation of predicted values from experimental values. For developing variable turblent Schmidt number model, it is

necessary to adopt high quality benchmark experiment for determining the parameters in the developed model. The experiment from Xu and Chen (2012) provided good data base for this aim.

2.8 Conclusion

To summarize, the main measurement techniques in studying airflow in aircraft cabin include hot wire and hot sphere anemometers, PSV, PTV, PIV, etc. In some cases, two or three measurement methods were combined to obtain more reliable results. Standard $k-\varepsilon$ model, RNG $k-\varepsilon$ model and LES were used in a lot of numerical simulations of air distribution in aircraft cabin. On the simulation of indoor jet flows and stratified flows, DNS method was too expensive to be adopted in most engineering circumstances. Two equation ($k-\varepsilon$ model, $k-\omega$ model, etc.), seven equation RANS models, and LES were more commonly used in the investigation of jet flow and stratified flow problems. Quantitative comparison was suggested in the evaluation of model performances. Commonly used statistical parameters were fractional bias, mean square error, percentage of points within a factor of 2, geometric mean and geometric variance. In addition, literature shows that in stratified flow simulations, Sc_t value is of great significance on the prediction of scalar fields, and it is necessary to model the its value based on local flow structure. Finally, in the CFD simulation of gasper jet, incorporating the realistic gasper geometry will bring more reliable results on the flow characteristics and the evaluation of its effect on decontamination in a passenger's breathing zone.

CHAPTER 3. NUMERICAL SIMULATION OF JET FLOWS UNDER DIFFERENT TURBULENCE AND STRATIFICATION LEVELS

This section describes the most prevalent turbulence models used for predicting stratified jets, the experimental data used for validating the models and the numerical algorithm used in solving the turbulence model. Mean velocity, TKE and turbulent shear stress were considered in the comparison of model performances. MSE was used to quantify the evaluation.

3.1 Governing Equations

Stratified flow with a small density difference can be described by continuity equation

$$\frac{\partial \rho}{\partial t} + \frac{\partial}{\partial x_i}(\rho u_i) = 0, \quad \text{(i=1,2,3)} \tag{3.1}$$

momentum equation

$$\rho \frac{\partial u_j}{\partial t} + \rho u_i \frac{\partial u_j}{\partial x_i} = -\frac{\partial p}{\partial x_j} + \mu \frac{\partial^2 u_j}{\partial x_i \partial x_i} + \rho g_j, \quad \text{(i=1,2,3)} \tag{3.2}$$

and species (scalar) transport equation

$$\frac{\partial}{\partial t}(\rho C_j) + \rho u_i \frac{\partial C_j}{\partial x_i} = -\frac{\partial J_j}{\partial x_i}, \text{ (i=1,2,3)} \tag{3.3}$$

The details of the modeling for the equations are shown in Table 3.1.

In a RANS simulation, a specific flow variable is decomposed into mean components and fluctuating components: $u_i = \bar{u}_i + u_i'$, $\phi = \bar{\phi} + \phi'$, where $\overline{u_i}$ and u_i' are the mean and fluctuating velocity components, and $\overline{\phi}$ and ϕ' are the mean and fluctuating scalar components. The mean components are solved from the RANS equations. On the other side, in LES, the flow variables are filtered by a low-pass filtering operation with a chosen filter width (corresponding to the grid spacing used in the computation). As a result, the large eddies are solved from filtered Navier-Stokes equations, and the influence of the unresolved (sub-grid scale, SGS) eddies is described by SGS models.

This investigation used the following prevalent turbulent models: the standard $k-\varepsilon$ model (Launder and Spalding 1972), RNG $k-\varepsilon$ model (Yakhot and Orszag 1986), realizable $k-\varepsilon$ model (Shih et al. 1994), standard $k-\omega$ model (Wilcox, D.C. 1998), SST $k-\omega$ model (Menter 1994), and RSM model (Gibson and Launder 1978; Launder 1989; Launder et al. 1975). Since LES has often been believed to yield a more accurate prediction than RANS, LES has also been examined using the Smagorinsky-Lilly model (Smagorinsky 1963). The transport equations for any mean parameter in the turbulence models can be expressed in a general form (White and Corfield 1991; Patankar 1980):

$$\rho \frac{\partial \bar{\phi}}{\partial t} + \rho \bar{u}_i \frac{\partial \bar{\phi}}{\partial x_i} - \frac{\partial}{\partial x_i}\left[\Gamma_{\phi,eff} \frac{\partial \bar{\phi}}{\partial x_i} \right] = S_\phi \tag{3.4}$$

where ϕ represents a specific variable, $\Gamma_{\phi,eff}$ the coefficient of effective diffusion, and S_ϕ the source term. Table 3.1 summarizes the choices of $\Gamma_{\phi,eff}$, S_ϕ and the corresponding constants in the governing equations and turbulence modeling equations used in the current investigation.

Table 3.1. Coefficients of Equation (3.4).

Equation or model		ϕ	$\Gamma_{\phi,eff}$	S_ϕ	Constants
Reynolds averaged variables	Continuity	1	0		
	Momentum	u_j	$\mu+\mu_t$	$-\frac{\partial p}{\partial x_i}+\frac{\partial}{\partial x_j}\left[(\mu+\mu_t)\frac{\partial u_j}{\partial x_i}\right]$	
	Species	C	$\mu/\sigma_C+\mu_t/\sigma_{C,t}$	S_C	$\sigma_{C,t}$: turbulent Schmidt number
2-equation	(1) Standard $k-\varepsilon$	k	$\mu+\mu_t/\sigma_k$	$G_k+G_b-\rho\varepsilon$	$\mu_t=\rho C_\mu\frac{k^2}{\varepsilon}$, $G_k=\mu_t S^2$, $S=\sqrt{2S_{ij}S_{ij}}$, $G_b=\beta g_i\frac{\partial\mu_t}{\partial\sigma_{T,t}}\frac{\partial\overline{T}}{\partial x_i}$, $C_{1\varepsilon}=1.44$, $C_{2\varepsilon}=1.92$, $C_\mu=0.09$, $\sigma_k=1.0$, $\sigma_\varepsilon=1.3$
		ε	$\mu+\mu_t/\sigma_\varepsilon$	$C_{1\varepsilon}G_k\frac{\varepsilon}{k}-C_{2\varepsilon}\rho\frac{\varepsilon^2}{k}$	
	(2) Realizable $k-\varepsilon$	k	$\mu+\mu_t/\sigma_k$	$G_k+G_b-\rho\varepsilon$	$\mu_t=\rho C_\mu\frac{k^2}{\varepsilon}$, $G_k=\mu_t S^2$, $S=\sqrt{2S_{ij}S_{ij}}$,

Table 3.1. Continued.

Equation or model		ϕ	$\Gamma_{\phi,eff}$	S_ϕ	Constants
2-equation	(2) Realizable $k-\varepsilon$	ε	$\mu+\mu_t/\sigma_\varepsilon$	$\rho C_1 S\varepsilon - \rho C_2 \frac{\varepsilon^2}{k+\sqrt{\upsilon\varepsilon}}$	$G_b = \beta g_i \frac{\partial \mu_t}{\partial \sigma_{T,t}} \frac{\partial \overline{T}}{\partial x_i}$, $C_1 = \max\left[0.43, \frac{\eta}{\eta+5}\right]$, $\eta = S\frac{k}{\varepsilon}$, $C_\mu = \frac{1}{A_0 + A_s \frac{kU*}{\varepsilon}}$, $U* \equiv \sqrt{S_{ij}S_{ij} + \Omega_{ij}\Omega_{ij}}$, $C_{1\varepsilon} = 1.44$, $C_2 = 1.9$, $\sigma_k = 1.0$, $\sigma_\varepsilon = 1.2$
	(3) RNG $k-\varepsilon$	k	$\mu+\mu_t/\sigma_k$	$G_k + G_b - \rho\varepsilon$	$\mu_t = \rho C_\mu \frac{k^2}{\varepsilon}$, $G_k = \mu_t S^2$, $S = \sqrt{2S_{ij}S_{ij}}$, $G_b = \beta g_i \frac{\partial \mu_t}{\partial \sigma_{T,t}} \frac{\partial \overline{T}}{\partial x_i}$, $R_\varepsilon = \frac{C_\mu \rho \eta^3 (1-\eta/\eta_0)}{1+\beta\eta^3} \frac{\varepsilon^2}{k}$, $\eta \equiv Sk/\varepsilon$, $\eta_0 = 4.38$, $\beta = 0.012$, $C_{1,\varepsilon} = 1.42$, $C_{2,\varepsilon} = 1.68$, $C_\mu = 0.0845$, $\sigma_k = 1.0$, $\sigma_\varepsilon = 1.3$
		ε	$\mu+\mu_t/\sigma_\varepsilon$	$C_{1\varepsilon} G_k \frac{\varepsilon}{k} - C_{2\varepsilon}\rho\frac{\varepsilon^2}{k} - R_\varepsilon$	

Table 3.1. Continued.

Equation or model		ϕ	$\Gamma_{\phi,eff}$	S_ϕ	Constants
2-equation	(4) Standard $k-\omega$	k	$\mu+\mu_t/\sigma_k$	G_k-Y_k	$\mu_t=\alpha^*\frac{\rho k}{\omega},\ \alpha^*=\begin{cases} High-\mathrm{Re}: \alpha^*_\infty=1 \\ Low-\mathrm{Re}: \alpha^*_\infty\left(\frac{\alpha^*_0+\mathrm{Re}_t/R_k}{1+\mathrm{Re}_t/R_k}\right)\end{cases}$, $\mathrm{Re}_t=\frac{\rho k}{\mu\omega}, R_k=6, \alpha^*_0=\frac{\beta_i}{3}\ \beta_i=0.072, G_k=\mu_t S^2$, $G_\omega=\alpha\frac{\omega}{k}G_k, Y_k=\rho\beta^* f_{\beta^*}k\omega, Y_\omega=\rho\beta f_\beta\omega^2$, $\beta^*_\infty=0.09, \sigma_k=2.0, \sigma_\omega=2.0$
		ω	$\mu+\mu_t/\sigma_\omega$	$G_\omega-Y_\omega$	
	(5) SST $k-\omega$	k	$\mu+\mu_t/\sigma_k$	G_k-Y_k	$\mu_t=\frac{\rho k}{\omega}\frac{1}{\max\left[\frac{1}{\alpha^*},\frac{SF_2}{a_1\omega}\right]}, \sigma_k=\frac{1}{F_1/\sigma_{k,1}+(1-F_1)/\sigma_{k,2}}$, $\sigma_\omega=\frac{1}{F_1/\sigma_{\omega,1}+(1-F_1)/\sigma_{\omega,2}}, G_k=\mu_t S^2, G_\omega=\frac{\alpha}{\nu_t}G_k$, $G_k=\min(G_k,10\rho\beta^* k\omega), Y_k=\rho\beta^* k\omega, Y_\omega=\rho\beta\omega^2$, $\sigma_{k,1}=1.176, \sigma_{\omega,1}=2.0, \sigma_{k,2}=1.0, \sigma_{\omega,2}=1.168$, $a_1=0.31$
		ω	$\mu+\mu_t/\sigma_\omega$	$G_\omega-Y_\omega$	

Table 3.1. Continued.

Equation or model		ϕ	$\Gamma_{\phi,eff}$	S_ϕ	Constants
7-equation	(6) RSM	$\overline{u_j' u_k'}$	$\mu+\mu_t/\sigma_i$	$P_{jk}+G_{jk}+\phi_{jk}-\varepsilon_{jk}$	$P_{jk}=-\rho\left(\overline{u_j' u_i'}\frac{\partial u_k}{\partial x_i}+\overline{u_k' u_i'}\frac{\partial u_j}{\partial x_i}\right)$, $G_{jk}=-\rho\beta\left(g_j\overline{u_k'\theta}+g_k\overline{u_j'\theta}\right)$, $\phi_{jk}=\overline{p\left(\frac{\partial u_j'}{\partial x_k}+\frac{\partial u_k'}{\partial x_j}\right)}$, $\varepsilon_{jk}=2\mu\frac{\partial u_j'}{\partial x_i}\frac{\partial u_k'}{\partial x_i}$
LES	(7) LES (Smagorinsky-Lilly)	1	0		
		u_j	μ	$-\frac{\partial\overline{p}}{\partial x_j}-\frac{\partial\tau_{ij}}{\partial x_j}$	$\tau_{ij}=\mu_t\left(\frac{\partial\overline{u}_i}{\partial\overline{x}_j}+\frac{\partial\overline{u}_j}{\partial\overline{x}_i}\right)+\frac{1}{3}\rho\tau_{kk}\delta_{ij}$, $\mu_t=\rho L_s^2\sqrt{2\overline{S}_{ij}\overline{S}_{ij}}$

3.2 Experimental Data of Stratified Jets

Since the turbulence modeling used approximations, it is essential to validate the computational results using experimental data. The experimental data from a stratified jet (Xu and Chen 2012) were used as benchmarks in the present study to validate and develop the models. Figure 3.1 shows the schematic of the experiment, and four sets of data were acquired. In two unstratified cases ("high-Re" and "low-Re"), the fluid discharged from the jet nozzle had the same density as the fluid in the tank. In two stratified cases ("high-Ri" and "low-Ri"), the fluid injected into the tank was of higher density than the fluid in the tank, leading to density stratification. In order to quantify the degree of stratification, the Richardson number was employed: $Ri_0 = \Delta\rho_0 Dg/(\rho U_0^2)$, where $\Delta\rho_0$, D, U_0 are the characteristic density differences, length scale, and velocity, respectively. In the experiment, both velocity and density fields were measured with the combined PIV and PLIF system. With the velocity and density data, Xu and Chen examined averaged parameters, Reynolds stresses, vertical density flux, turbulent kinetic energy budget, etc., within central vertical plane. Measurements were aconducted in both unstratified and stratified cases, as summarized in Table 3.2. The current investigation mainly focuses on the numerical calculations in stratified cases. Average velocity, average density, turbulent kinetic energy and Reynolds stress values were examined in the present study.

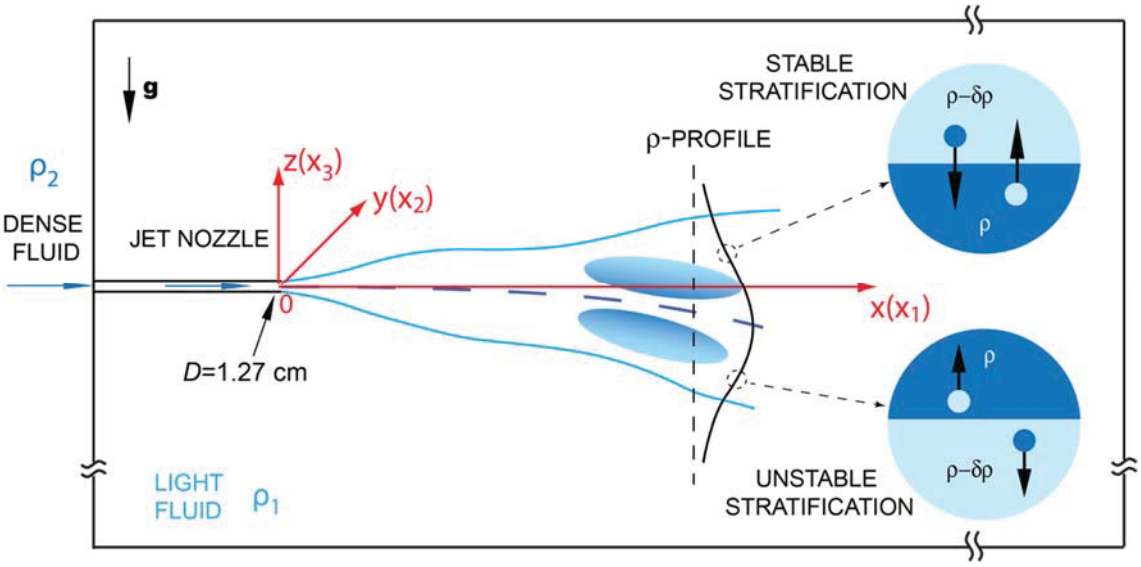

Figure 3.1. Setup of the stratified flow experiment (Xu and Chen 2012).

Table 3.2. Parameters at the jet nozzle of the four experimental cases.

Case	High-Re	Low-Ri	Low-Re	High-Ri
Jet velocity (mean) $U_0(m/s)$	1.88	1.88	0.24	0.24
Turbulent intensity $I = u/U_0$	3.3%	6.0%	3.4%	3.5%
Initial density difference $\Delta\rho_0/\rho_s$	0	0.5%	0	0.5%
Reynolds number $\mathrm{Re}_0 = \rho_s U_0 D/\mu$	24,000	24,000	3,200	3,200
Richardson number $Ri_0 = \Delta\rho_0 Dg/(\rho_s U_0^2)$	0	0.0002	0	0.01

In this horizontal stratified jet, both stable and unstable stratification regions exist, as shown in Fig. 3.1. Stable stratification was formed where $d\bar{\rho}/dz > 0$ and turbulence were weakened by the buoyancy effect. Unstable stratification was formed where $d\bar{\rho}/dz < 0$ and turbulence was enhanced by the buoyancy effect. The measurements enable comparative studies in both stable and unstable stratification regions.

3.3 Numerical Simulations of the Stratified Jets

Our numerical simulation of the stratified jet flow used the following assumptions: (1) Since the averaged flow field was symmetric with respect to the central vertical plane (y=0), half of the domain was used in the RANS simulations. In LES, the whole domain should be used to resolve the three dimensional unsteady flow motions. (2) A solid cylinder was deployed in the tank to simulate the existence of the jet nozzle, and the velocity and scalar profiles at the jet exit were prescribed as boundary conditions. Fig. 2a shows the dimensions of the computation domain, which is exactly the same size as in the experiment. Fig. 3.2b, 3.2c and 3.2d present the mesh of the CFD model for RANS cases. The mesh structure for LES simulation is very similar to that shown in Fig. 3.2, but the grids were much finer, as detailed below.

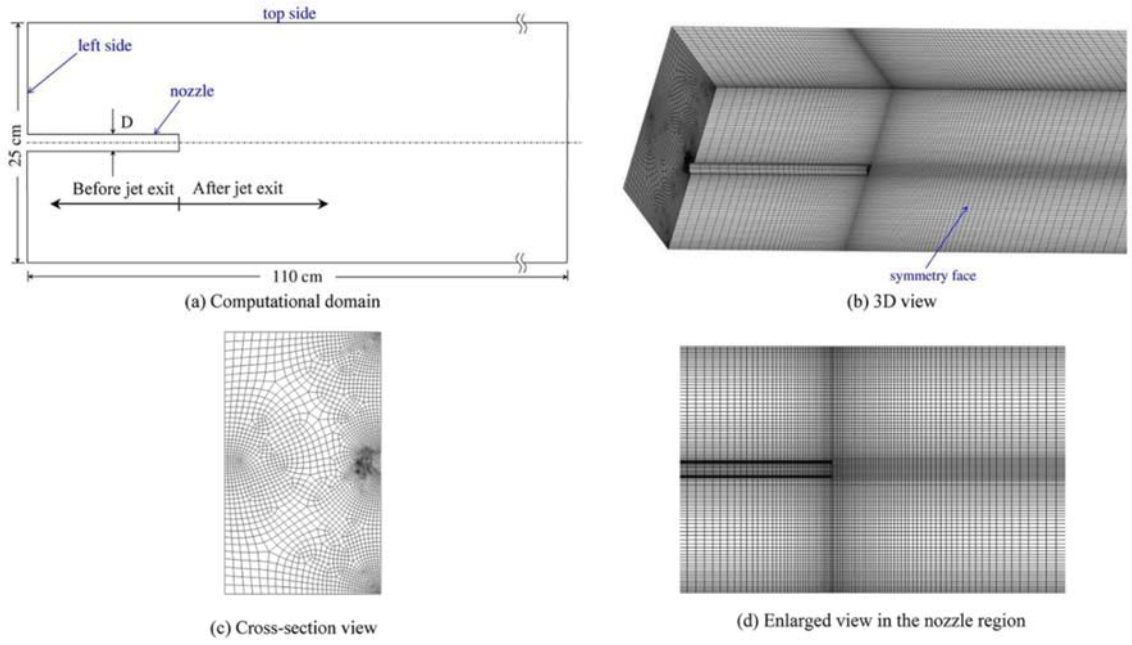

Figure 3.2. Computational domain and mesh structure for stratified jet simulation.

This study adopted a non-uniform grid size method for the meshing. The grid was the finest at the jet nozzle and gradually increased from the nozzle. To check grid independence, RANS simulations (using the standard $k-\varepsilon$ model) of the Low-Ri case were conducted on three different grids: 214,990, 431,280, and 811,190 grids, respectively, representing coarse, medium, and fine grids. However, different numbers of cells were used on the jet axes and cross-sections (vertical to axes) of the fluid domain. The table in Fig. 3.3 describes the detailed differences of the three grids. Fig. 3.3 also shows the velocity profiles along the centerline from these three grid systems. The results from the coarse and medium grids showed significant differences, while the results from the medium and fine grids almost collapsed. This suggests that the medium grid led to grid-independent results and the grid was used in the following RANS simulations. Since LES needs to use the entire domain and it typically requires finer meshes, the grid independence test for LES was conducted separately in a similar way. The number of grids for LES was finalized at 1,624,130.

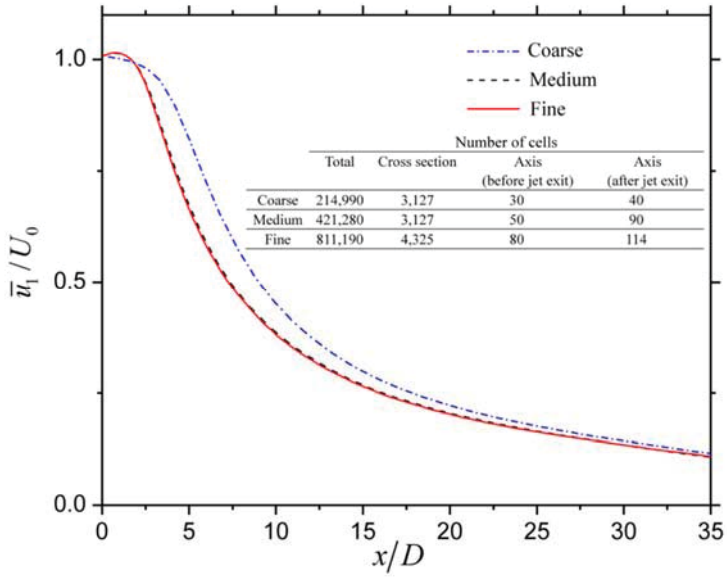

Figure 3.3. The jet centerline velocity predicted by RANS from different grids.

This study employed a numerical solver in ANSYS Fluent 14.0 to solve Equations (3.1) to (3.3) to obtain the flow and scalar fields. Pressure-velocity was coupled using the SIMPLE scheme. The second-order upwind scheme was used to discretize the momentum, turbulent kinetic energy, and species term. In order to assure accuracy, the second order implicit method was employed for the transient formulation. Unsteady simulations were adopted with time step 0.005s. A sensitivity study was also done on time step size by confirming that a smaller time step did not change the simulation results a lot. At each time step, 30 iterations were conducted. Within each time step, x, y and z velocity residuals dropped by 4 orders of magnitude; at the end of each time step size, and scaled species residual decreased to 10^{-7} . For LES simulations, 3-second time interval was used for data collecting and averaging in obtaining averaged values from instantaneous parameters.

At the jet exit, the velocity and scalar (mass fraction) profiles were prescribed according to the experimental data. The right boundary of the calculation domain was defined as a pressure-outlet, which served as an outlet for the flow. (For the pressure-outlet boundary, when gravity was enabled in the calculation, the increase of pressure due to gravity was considered automatically.) In the experiment, the topside was the interface between the fluid and the atmosphere, and it was assumed shear force was zero on the interface. Thus zero-shear (symmetry) boundary condition was defined for the top boundary in the present simulation. For other boundaries, no-slip boundary conditions were specified.

3.4 Mean Square Error (MSE) Used for Model Performance Comparison

As suggested by Britter and Schatzmann (2007), quantitative comparison with experimental data is a good method to evaluate the performances of various turbulence models. Thus MSE (Mean Squared Error) (Lehmann and Casella 1998) was used to describe the degree of deviation of predicted values from experimental values in this study. MSE is defined as

$$MSE = \frac{1}{N}\sum_{i=1}^{N}(X_{p,i} - X_{m,i})^2 , \qquad (3.5)$$

where $X_{p,i}$ is the predicted value at i-th location, $X_{m,i}$ is the measured value at i-th location and N is the number of locations compared.

3.5 Results

Fig. 3.4 shows the velocity contours and streamlines for both weak stratification (low-Ri) and strong stratification (high-Ri) cases. Dash lines represent the boundaries of computational domain. The present study evaluates the performance of six RANS models and LES in stratified flow, under the two cases. For each case, first order moment (mean velocity) and second order moments (turbulent kinetic energy and Reynolds stresses) were compared with experimental data at fully-developed downstream locations (x=20D for low-Ri case and x=10D for high-Ri case, respectively). The turbulent kinetic energy is

$$TKE = \frac{1}{2}\left(\overline{u_1'u_1'} + \overline{u_2'u_2'} + \overline{u_3'u_3'}\right) \tag{3.6}$$

and a shear Reynolds stress, $\overline{u_1'u_3'}$, were compared with the experimental data.

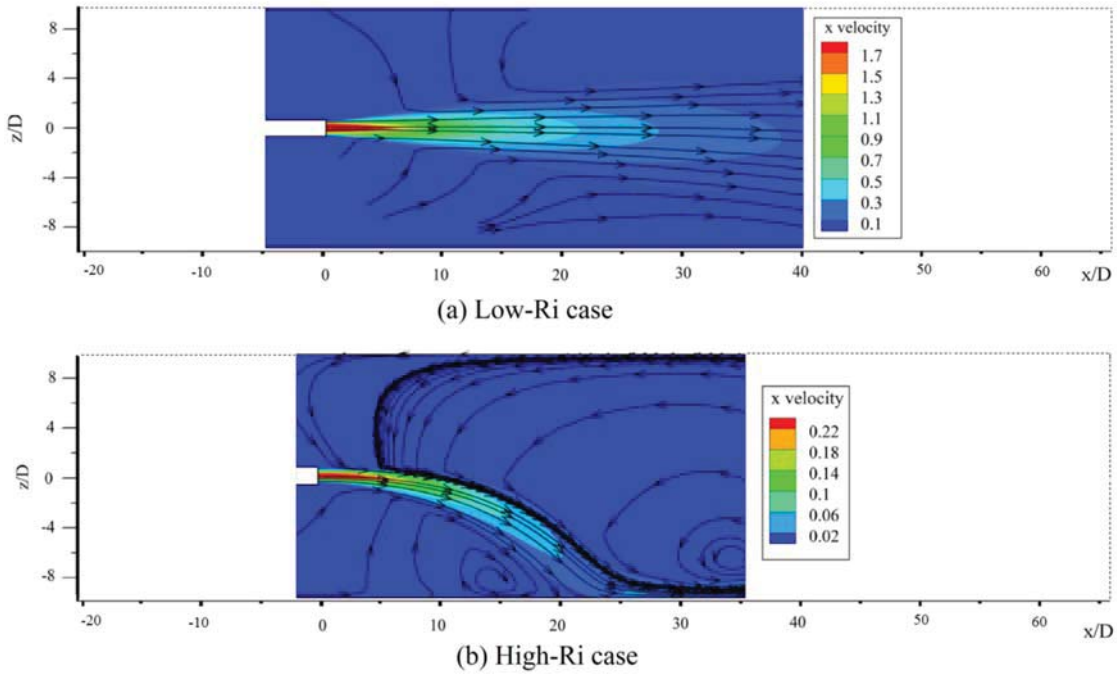

Figure 3.4. Velocity contours and streamlines from the simulation results (m/s).

3.5.1 Mean Velocity

In the horizontally introduced stratified jet, its centerline deviates from the horizontal direction due to the buoyancy effect, as demonstrated in Fig.3.5. To quantify the degree of this deviation, z_c was defined such that $U_c(x)=\bar{u}_1(x,0,z_c)$, where $U_c(x)$ was the peak value at downstream location x. Meanwhile, to characterize the jet expansion, two half-width locations, $z_{+1/2}$ and $z_{-1/2}$ were defined in stable and unstable regions, respectively:

$$\bar{u}(x,0,z_{+1/2})=\bar{u}(x,0,z_{-1/2})=U_c/2 \tag{3.7}$$

The corresponding half-widths of the jet in stable and unstable regions were defined respectively:

$$r_{-1/2} = z_c - z_{-1/2} \ , \ r_{+1/2} = z_{+1/2} - z_c \tag{3.8}$$

The self-similarity characteristics of a homogenous round jet, $\bar{u}/U_c$ vs. $r / r_{1/2}$, can be found in many other studies, e.g., Pope (2001).

Fig. 3.6 shows the self-similarity curves from the experimental data and simulation results. Due to the stratification, $_z$ coordinate was normalized as $(z-z_c)/r_{1/2}$, where $r_{1/2} = (r_{-1/2} + r_{+1/2})/2$. In the low-Ri case (Fig. 7a), the simulation results agree well with the experimental data in the stable stratification region, but in the unstable stratification region, a discrepancy was observed for certain turbulence models. Based on the MSE values from Table 3.3, the SST $k-\omega$ model, standard $k-\varepsilon$ model and RNG $k-\varepsilon$ model yielded the best performances, while the results from the other models were still acceptable. This shows that when the stratification was weak and the turbulence effect was dominant (Re=24,000), these models could yield an accurate prediction of the mean velocity.

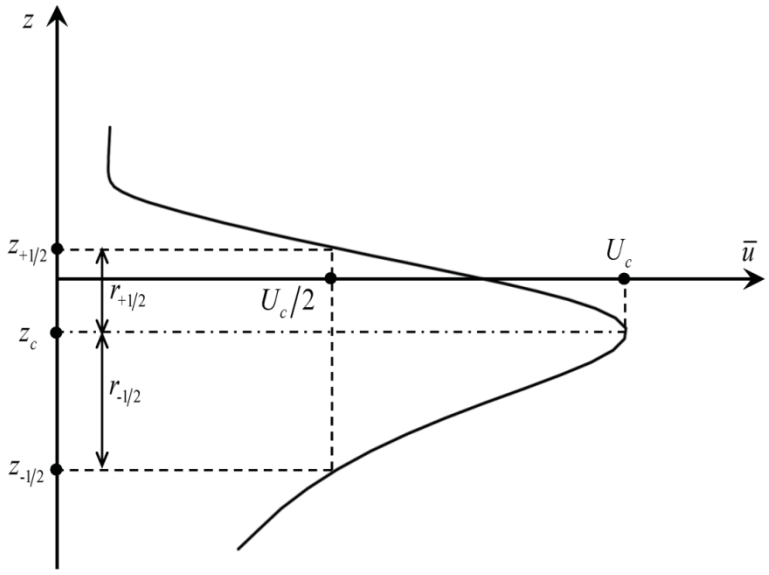

Figure 3.5. Mean velocity profile of a typical horizontal stratified jet.

In the high-Ri case (Fig. 3.6b), the stratified jet bends more quickly than in the low-Ri case. Overall, the performances of the turbulence models were worse in the high-Ri case than in the low-Ri case. This indicates that most of the tested models work better in high Reynolds number flows than in low or transitional Reynolds number flows. The prediction accuracy in the stable stratification region was different from the one in the unstable stratification region. In the stable stratification region, all the turbulence models gave acceptable predictions of the mean velocity. However, in the unstable stratification region, large discrepancies from the experimental results were observed in the results from the RSM model and LES. Although the RSM model solved transport equations for Reynold stresses, which can be helpful for predicting second order flow characteristics, it was deficient in predicting the mean velocity when the stratification was strong. The LES result in the unstable stratification region deviated even more from the experimental data than the RSM result, possibly due to the problem of the Smogrinsky-Lilly model for flow

in a transitional region. As indicated by Voke (1996), the coefficients of the Smagorinsky-Lilly model are proportional to the square of the grid scale, and vanish too slowly when the Reynolds number is low. As a result, LES with the Smagorinsky-Lilly model overpredicts the subgrid eddy-viscosity. Our results show once again that the prediction of flow features in the unstable stratification region was more difficult than in the stable stratification region. The MSE values showed that SST $k-\omega$ model gave the best mean velocity profile among all the models tested, similar to the tests for the low-Ri case. One important advantage of the SST $k-\omega$ model is that a low Reynolds number correction can be used to damp the turbulent viscosity in low Reynolds number simulations.

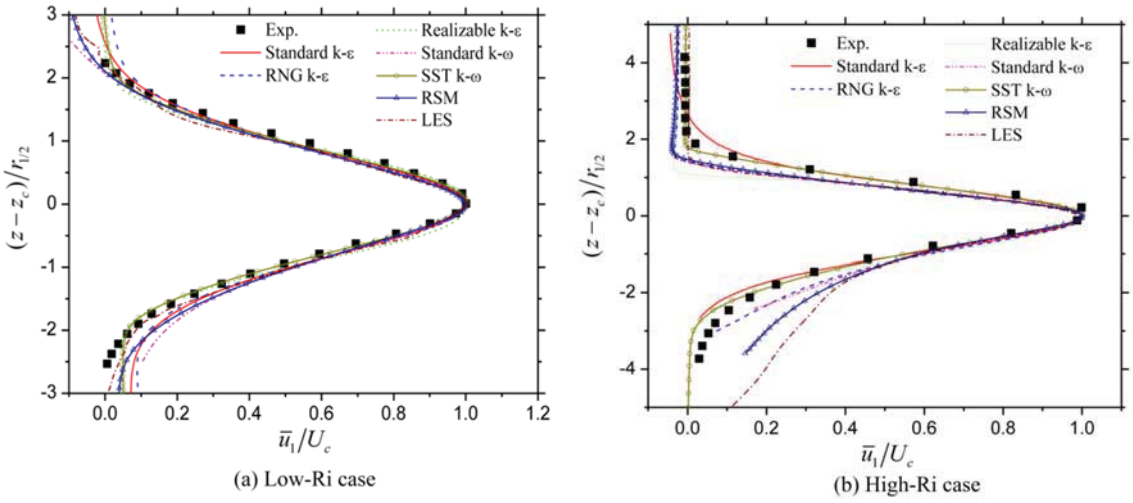

Figure 3.6. Self-similarity curves of mean velocity.

Table 3.3. Mean squared errors of mean velocity self-similarity values

	MSE (Mean Squared Error)						
	Standard $k-\varepsilon$	RNG $k-\varepsilon$	Realizable $k-\varepsilon$	Standard $k-\omega$	SST $k-\omega$	RSM	LES
Low-Ri	1.86×10^{-3}	1.96×10^{-3}	1.99×10^{-3}	3.93×10^{-3}	6.10×10^{-4}	2.79×10^{-3}	2.45×10^{-3}
High-Ri	1.62×10^{-3}	7.39×10^{-3}	1.03×10^{-2}	8.18×10^{-3}	8.47×10^{-4}	1.15×10^{-2}	1.76×10^{-2}

3.5.2 Turbulent Kinetic Energy

Fig. 3.7 shows the predicted TKE at a downstream location in low-Ri and high-Ri cases, and Table 3.4 illustrated the MSE values under various models. For the low-Ri case (Fig. 8a), among all the two-equation models, the SST $k-\omega$ model led to the best results. The three variations of $k-\varepsilon$ models also captured the general trend of the TKE profile. However, standard $k-\omega$ significantly underpredicted TKE at the core region of the jet (-2<z/D<2). Compared to the standard $k-\omega$ model, the SST $k-\omega$ model modified the turbulent viscosity formulation to account for the transport effects of the principal turbulent shear stress. Since the stratified jet flow was a typical shear stress flow, this is why the SST $k-\omega$ model yielded a significantly better prediction. The RSM model also led to acceptable prediction of TKE. The experimental result shows a “dent” around the center of the jet, and the RSM was the only model that could predict it. On the other hand, LES did not produce satisfactory results as expected because the SGS model tested in the present study may be the source of the prediction error.

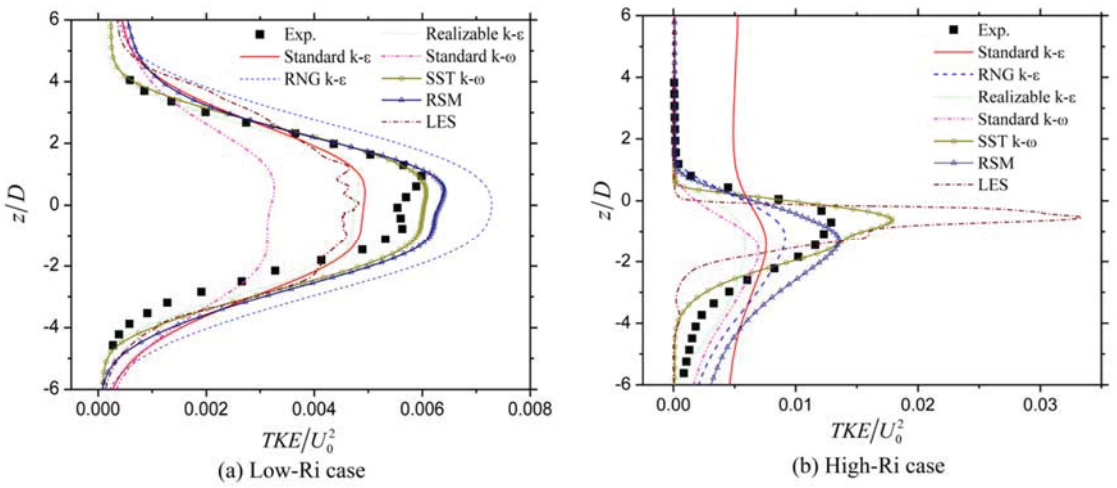

Figure 3.7. Turbulent kinetic energy distributions.

Table 3.4. Mean squared errors of turbulent kinetic energy distributions.

	MSE (Mean Squared Error)						
	Standard $k-\varepsilon$	RNG $k-\varepsilon$	Realizable $k-\varepsilon$	Standard $k-\omega$	SST $k-\omega$	RSM	LES
Low-Ri	6.26×10^{-7}	2.62×10^{-6}	4.26×10^{-7}	2.64×10^{-6}	3.94×10^{-7}	6.69×10^{-7}	8.39×10^{-7}
High-Ri	1.59×10^{-5}	4.64×10^{-6}	1.05×10^{-5}	1.17×10^{-5}	3.05×10^{-6}	5.82×10^{-6}	2.62×10^{-5}

Fig. 3.7b compares the TKE profiles predicted with the experimental data in the high-Ri case. Due to the strong stratification in the high-Ri case, the TKE profile was asymmetric and the peak deviated downwards. Similar to in the low-Ri case, the RSM and SST $k-\omega$ models gave good predictions of the TKE distribution at locations close to jet axis, and SST $k-\omega$ model gave the best overall TKE predictions. LES overpredicted significantly the TKE, which may be attributed to the deficiency of the Smagorinsky-Lilly model in low Reynolds number flows. Overall, the predictions of TKE in this case were not as accurate as those in the low-Ri case, which was similar for the mean velocity.

3.5.3 Shear Stress

Figure 3.8 shows the comparison between shear stresses. From Table 3.5, for the low-Ri case, the models that perform well in predicting TKE, the SST $k-\omega$ model, and the RSM model, also gave good predictions of $\overline{u_1'u_3'}$, especially in stable stratification region. The RSM model solved the transport equation for Reynolds stresses, while other eddy viscosity models relied on the assumption that μ_t was isotropic, which is not true in stratified flows. Thus, the RSM model was better in predicting Reynolds stresses than mean velocities. Since the RNG $k-\varepsilon$ model can take the stratification effects (Moghaddasi-Naini et al. 1998) into account, it also performed well. For shear stress results, all predicted profiles captured the inverse-symmetric characteristic. However, the magnitude in the unstable stratification region was underpredicted compared with in the stable stratification region. This indicates that the simulations in the unstable stratification region were more difficult due to the complex physics of fluid in this region.

For the high-Ri case, the RNG $k-\varepsilon$ model still yielded the best prediction among all three $k-\varepsilon$ models, although its prediction performance in the unstable region was much worse than in the stable region. The SST $k-\omega$ model and RSM model also underpredicted the shear stress in the unstable stratification regions. However, these two models performed best when evaluated by the overall results. All the other RANS models underpredicted the stresses. LES overpredicted the shear stress in stable stratification region but underpredict it in unstable stratification region.

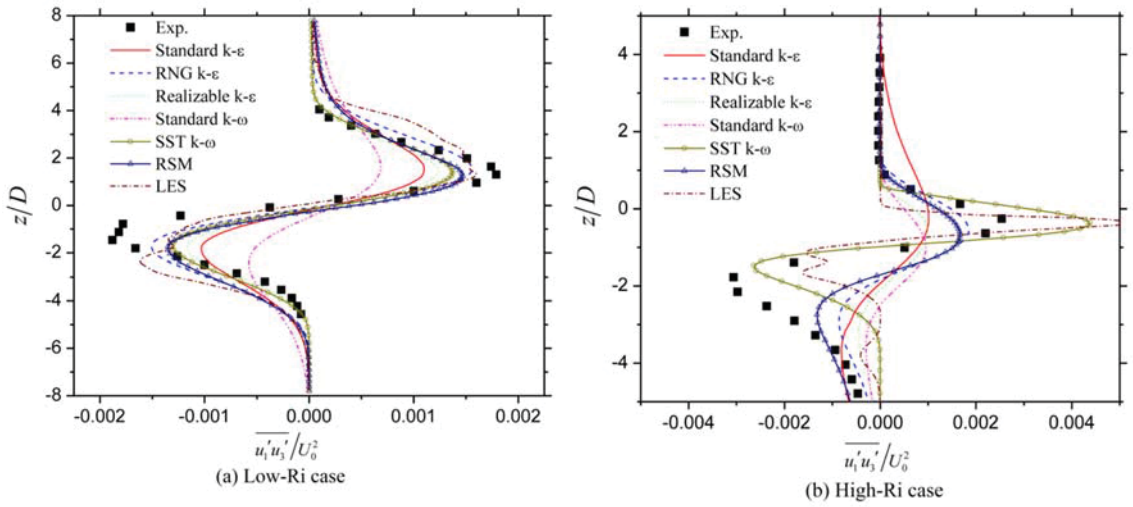

Figure 3.8. Shear Reynolds stress $\overline{u_1'u_3'}$ distributions.

Table 3.5. Mean squared errors of shear Reynolds stress distributions.

	MSE (Mean Squared Error)						
	Standard $k-\varepsilon$	RNG $k-\varepsilon$	Realizable $k-\varepsilon$	Standard $k-\omega$	SST $k-\omega$	RSM	LES
Low-Ri	2.73×10^{-7}	1.25×10^{-7}	2.05×10^{-7}	6.19×10^{-7}	1.42×10^{-7}	1.94×10^{-7}	1.91×10^{-7}
High-Ri	1.34×10^{-6}	1.13×10^{-6}	1.52×10^{-6}	1.86×10^{-6}	7.01×10^{-7}	9.29×10^{-7}	1.21×10^{-6}

3.5.4 Prediction of Vorticity in the Stratified Jets

Studying vorticity is important for characterizing the local flow structure. Fig. 3.9 shows the vorticy contours at the center vertical plane in the low-Ri and high-Ri cases predicted by the SST $k-\omega$ model and compares them to the experimental data. In the low-Ri case, the vorticity distribution was almost antimetric, and the boundary between negative and positive vorticity was basically the centerline when x/D<15. In the high-Ri case, in contrast, the boundary bent downwards with the increase of x/D. The vorticity in the stable stratification region was larger than in the unstable stratification region. Overall,

the vorticity distributions in both the weak and strong stratification jets were captured with acceptable accuracy. These results show again that the SST $k-\omega$ model can predict the stratified flow characteristics.

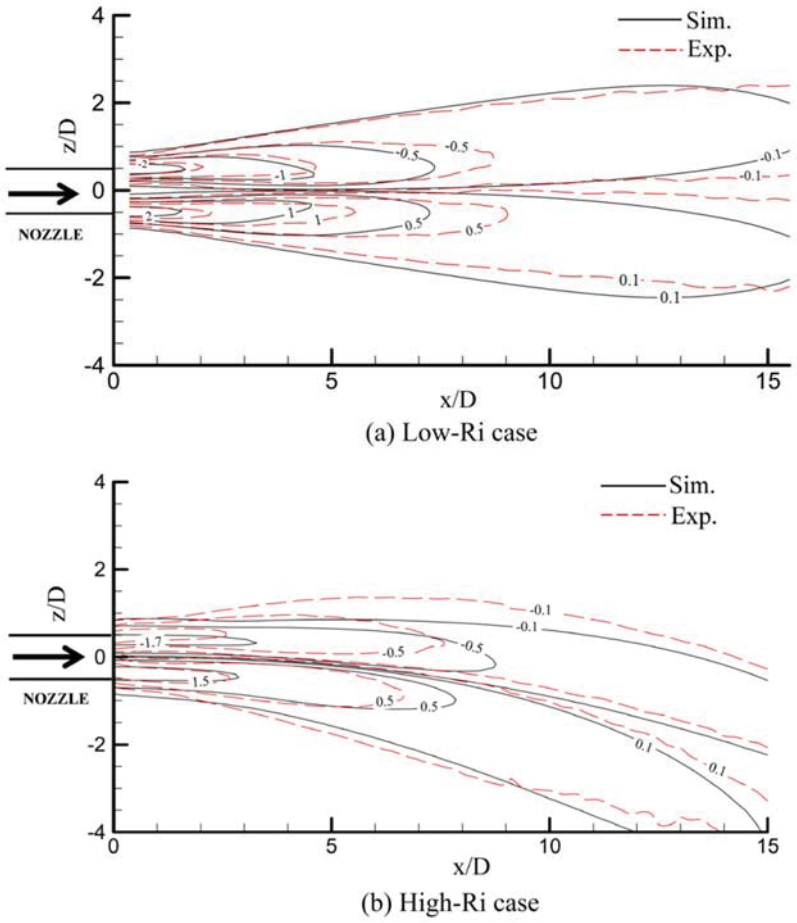

Figure 3.9. Vorticity (normalized as $\Omega_2 D/U_0$) contours in the low-Ri and high-Ri cases.

3.5.5 Entrainments in the Stratified Jets

The numerical simulations also enable us to analyze the entrainment in the stratified jets. The entrainment ratio is defined as $\frac{m}{m_0}$, where m_0 is the mass of fluid discharged from

the jet nozzle and m is the mass across a section perpendicular to the jet. Ricou and Spalding (1961) concluded that the entrainment ratio of a horizontal jet could be expressed by using an empirical formula: $\frac{m}{m_0} = 0.32(\frac{\rho_1}{\rho_0})^{\frac{1}{2}} \frac{x}{D}$, where ρ_0 is the density of the fluid discharged from the nozzle, and ρ_1 is the density of ambient fluid. In this study, we employed the SST $k-\omega$ model to predict the entrainment ratio and compared the results with those of the empirical formula.

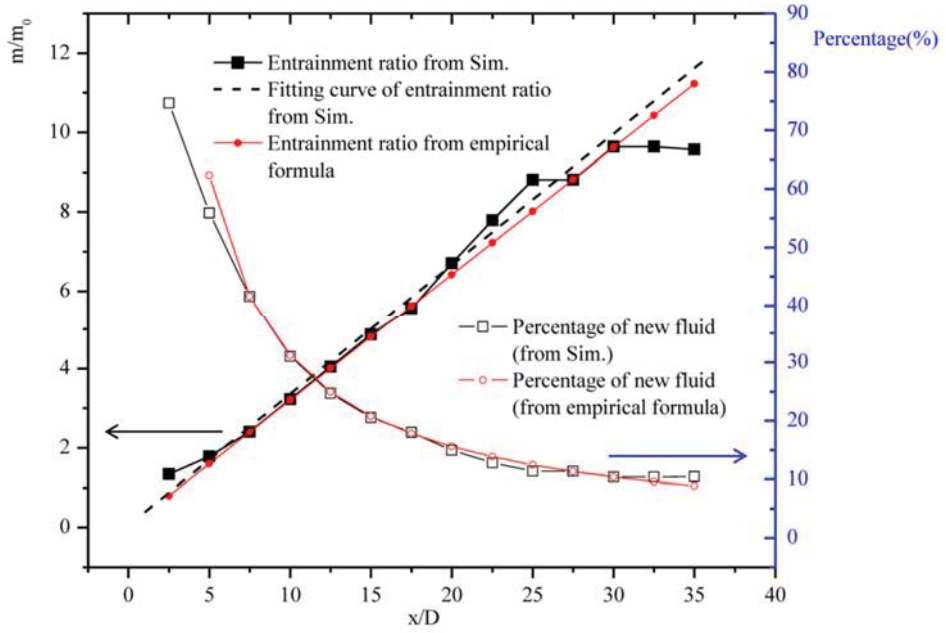

Figure 3.10. The entrainment ratio and the percentage of new fluid in the low-Ri case.

As shown in Fig. 3.10, both methods gave a good prediction for the entrainment ratio when x/D<30, where the increase of the entrainment ratio was proportitional to x/D. However, a large discrepancy was found where x/D>30. This was mainly due to the confinement of the fluid tank, which decreased the amount of entrainment. The empirical

formula assumed a perfect free-jet. Due to the entrainment, the percentage of fluid in the jet from the nozzle (called “new fluid”) decreased as x/D increased. When x/D>30, only about 10% of the fluid in the jet originated from the nozzle.

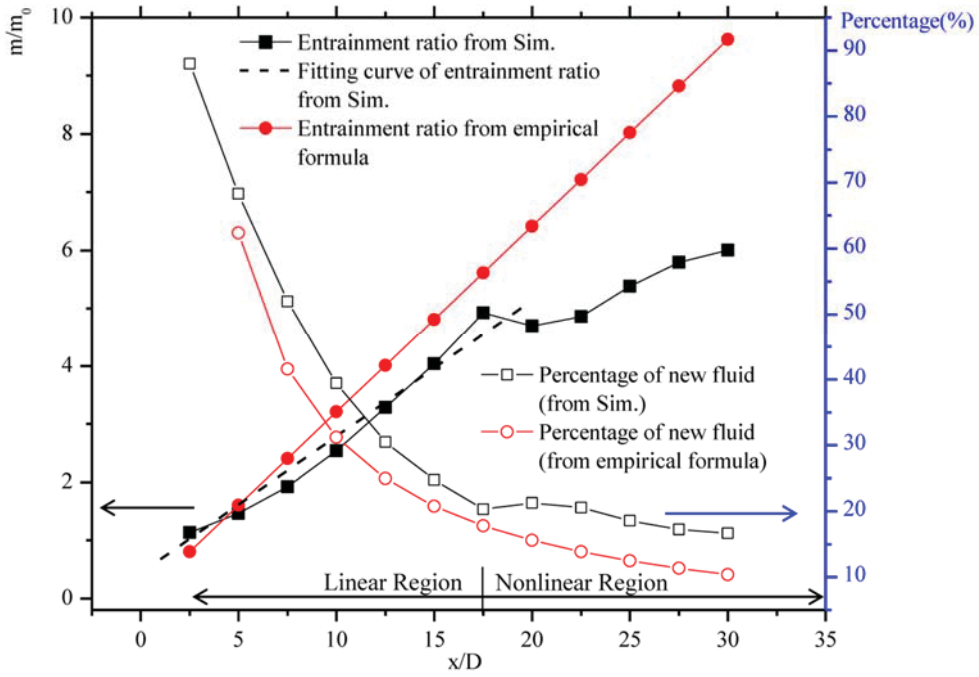

Figure 3.11. The entrainment ratio and the percentage of new fluid in the high-Ri case.

The entrainment in the high-Ri case was much more complex than in the low-Ri case. The entrainment ratio predicted by the SST $k-\omega$ model was smaller than that from the empirical formula. The reason is that the strong buoyancy effect in the high-Ri jet bent the jet heavily, which led to a decrease in the entrainment while the empirical formula assumed the buoyancy effect to be negligible. Therefore, the empirical formula should not be used for determining the jet entrainment with strong stratification. The numerical prediction in Fig. 3.11 shows that the entrainment ratio curve can be divided into a linear region and a nonlinear region. In the linear region, the entrainment ratio increased with

x/D with a linear coefficient of 0.235, a much smaller value than 0.32 in the empirical formula. The entrainment ratio in the nonlinear region increased more slowly than in the linear region due to the impingement of the jet at the tank wall, which decreased the entrainment amount.

3.6 Discussions

This study also evaluated the computation time by these seven models. All the six RANS models used the grid number of 431,280. Due to the high requirement for the grid resolution, the LES simulation used a much larger grid number of 1,624,130, which is about four times that for RANS simulations. The high-Ri case was used for comparison. All the simulations were tested on one node of a Linux-cluster with two 2.5 GHz Quad-Core AMD 2380 processors.

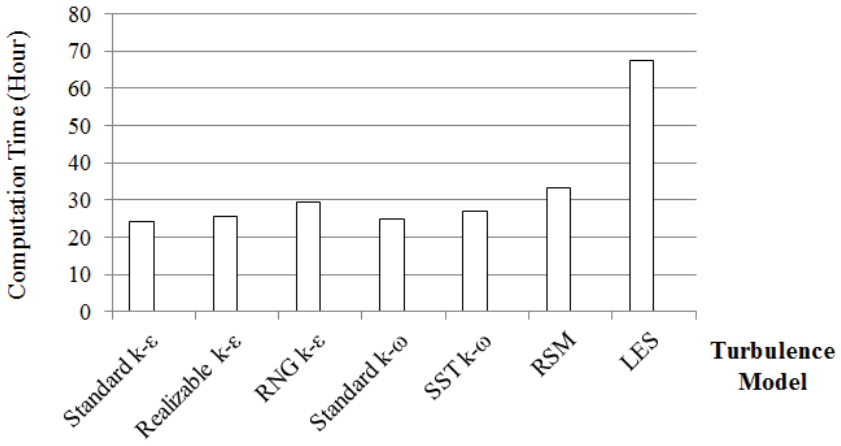

Figure 3.12. The computation time needed by different CFD models.

The calculation time for running a 12-second interval transient simultion with different models was recorded and plotted in Fig. 3.12. Among all the $k-\varepsilon$ models, the RNG $k-\varepsilon$ model required the longest computation time. The computation cost of the SST $k-\omega$ model was slightly higher than that of the standard $k-\omega$ model. Nevertheless, the computation costs of all five eddy-viscosity models were close. The computation cost of the RSM models was about 25% higher than the average of the eddy-viscosity models. This is understandable because the RSM model solved seven transport equations for turbulence parameters, while the eddy-viscosity model solved only two for turbulence. The LES simulation required about twice as much computation time as the RSM and almost three times the average computation time for the eddy-viscosity models. This is mainly attributed to the much larger number of grids used in the LES than in the RANS simulations.

Besides, in this chapter, the experimental dataset was obtained in tests where density variance existed. Density variant numerical simulation was conducted as well, and the simulatin results were used to evaluate the performances of different turbulence models in predicting stratified jet flows. However, it still needs to be further analyzed how much of the results and conclusions in current study can be analogized to cases where there is temperature variance and thermal plume exists.

3.7 Conclusion

This investigation quantitatively evaluated performances of 7 turbulence models using MSE. Vorticity distribution and entrainment were also simulated using CFD and compared with experimental results. The study led to the following conclusions:

(1) This investigation evaluated the performances of six RANS models and one LES model in predicting stratified flows. In the weakly stratified flow where the turbulent effect was dominant, all seven models could predict accurately the mean flow, but with large discrepancies in predicting the second-order flow characteristics. Overall, the RNG $k-\varepsilon$ and SST $k-\omega$ models performed very well, but the SST $k-\omega$ was the best. The superiority of LES was not observed in predicting the second-order flow characteristics.

(2) It was more difficult for the models to predict strongly stratified flow. All the models could still predict well the mean flow in the stable stratification region, but the RSM model and LES overestimated the velocity in the unstable stratification region. For predicting the second-order flow characteristics, the RSM, SST $k-\omega$ and RNG $k-\varepsilon$ models can be used, and the first two yielded the best overall results. The LES with the standard Smagorinksy model may not be suitable for the low Reynolds number transitional flows in this study. Therefore, LES does not always give better predicting results than RANS models, although it usually takes much longer time.

(3) The computation costs of the five eddy-viscosity models in RANS were comparable, but the RSM model required 25% more computing time, and the LES needed three times

more computing time. The adoption of the dynamic turbulent Schmidt number model used an additional 10% computing time.

(4) The CFD models can predict vorticity distributions in the stratified jets. The entrainment ratio can be calculated by the empirical formula for the weakly stratified jet but not for the strongly stratified jet. It is not suggested to use empirical formula to predict entrainment ratio when stratification is strong in jet flows.

CHAPTER 4. DYNAMIC SCHMIDT NUMBER MODELING IN STRATIFIED JET SIMULATION

This section describes the modeling of turbulent Schmidt number model (TSNM), as well as the effect of using different turbulent Schmidt number together with TSNM in CFD results. Scalar (density) distributions of different axial locations of jet are investigated in the comparisons.

4.1 Definition of Turbulent Schmidt Number

In mass diffusion process, Schmidt number Sc is defined as the ratio of momentum diffusivity and mass diffusivity: $Sc = \frac{\nu}{D}$, which measures the relative effectiveness of momentum and mass transport in diffusion (Cussler 2009; Incropera 2011). Similarly, in turbulent flows, turbulent Schmidt number is defined as (ANSYS 2011):

$$Sc_t = \frac{\nu_t}{D_t}, \tag{4.1}$$

where ν_t is eddy (or turbulent) viscosity, and D_t is eddy diffusivity.

4.2 Dynamic Schmidt Number Modeling

To simulate the stratified flows using eddy-viscosity-type models, the vertical momentum flux and density flux along the buoyancy direction were two key parameters being modelled by eddy viscosity ν_t and eddy diffusivity D_t:

$$\overline{u_1'u_3'} = -\nu_t \frac{\partial \overline{u}_1}{\partial x_3} \quad \text{and} \quad \overline{\theta' u_3'} = -D_t \frac{\partial \overline{\theta}}{\partial x_3} \tag{4.2}$$

As mentioned above, ν_t and D_t were related to turbulent Schmidt number $Sc_t = \nu_t / D_t$, which is usually chosen as a constant. Many aforementioned studies have shown the deficiency of such a simple model. For example, Xu and Chen (2012) demonstrated that density flux ($\overline{\theta' u_3'}$) was not only dependent on density gradient, but also on velocity gradient. The present study proposed a dynamic turbulent Schmidt number model that relates the local Sc_t with a local velocity gradient and scalar gradient. If one assumes in stratified flows that momentum flux and density flux are dependent on velocity gradient and density gradient and applies the Taylor expansion, i.e.,

$$\overline{u_1'u_3'} = f\left(\frac{\partial \overline{u}_1}{\partial x_3}, \frac{\partial \overline{\theta}}{\partial x_3}\right) = A_1 \frac{\partial \overline{u}_1}{\partial x_3} + A_2 \left(\frac{\partial \overline{u}_1}{\partial x_3}\right)^2 + \cdots + B_1 \frac{\partial \overline{\theta}}{\partial x_3} + B_2 \left(\frac{\partial \overline{\theta}}{\partial x_3}\right)^2 + \cdots \tag{4.3}$$

$$\overline{\theta' u_3'} = g\left(\frac{\partial \overline{u}_1}{\partial x_3}, \frac{\partial \overline{\theta}}{\partial x_3}\right) = C_1 \frac{\partial \overline{u}_1}{\partial x_3} + C_2 \left(\frac{\partial \overline{u}_1}{\partial x_3}\right)^2 + \cdots + D_1 \frac{\partial \overline{\theta}}{\partial x_3} + D_2 \left(\frac{\partial \overline{\theta}}{\partial x_3}\right)^2 + \cdots \tag{4.4}$$

where the A_i, B_i, C_i, and D_i were expansion coefficients (i=1, 2). When the first-order approximation was employed,

$$\overline{u_1'u_3'} \approx A_1 \frac{\partial \overline{u}_1}{\partial x_3} + B_1 \frac{\partial \overline{\theta}}{\partial x_3} \quad \text{and} \qquad \overline{\theta' u_3'} \approx C_1 \frac{\partial \overline{u}_1}{\partial x_3} + D_1 \frac{\partial \overline{\theta}}{\partial x_3} \tag{4.5}$$

Then the expression of Sc_t led to

$$Sc_t = \frac{\nu_t}{D_t} = \frac{\left(A_1 \frac{\partial \overline{u}_1}{\partial x_3} + B_1 \frac{\partial \overline{\theta}}{\partial x_3} \right) / \frac{\partial \overline{u}_1}{\partial x_3}}{\left(C_1 \frac{\partial \overline{u}_1}{\partial x_3} + D_1 \frac{\partial \overline{\theta}}{\partial x_3} \right) / \frac{\partial \overline{\theta}}{\partial x_3}} = \frac{A_1 + \frac{B_1}{\frac{\partial \overline{u}_1}{\partial x_3} / \frac{\partial \overline{\theta}}{\partial x_3}}}{D_1 + C_1 \frac{\partial \overline{u}_1}{\partial x_3} / \frac{\partial \overline{\theta}}{\partial x_3}} \tag{4.6}$$

Sc_t thus can be expressed as a function of $\frac{\partial \overline{u}_1}{\partial x_3} / \frac{\partial \overline{\theta}}{\partial x_3}$, or its normalized term $\frac{\partial \overline{u}_1^*}{\partial x_3^*} / \frac{\partial \overline{\theta}}{\partial x_3^*}$ ($x_3^* = \frac{x_3}{D}$, $\overline{u}_1^* = \frac{\overline{u}_1}{U_0}$, where D and U_0 are the characteristic length scale and characteristic velocity. By using Taylor's expansion again and denoting $t = \frac{\partial \overline{u}_1^*}{\partial x_3^*} / \frac{\partial \overline{\theta}}{\partial x_3^*}$, Sc_t can be expressed as

$$Sc_t = h(t) = \alpha_0 + \alpha_1 t + \alpha_2 t^2 + \cdots \tag{4.7}$$

where the model coefficients α_i's can be determined by the experimental data, as shown in Fig. 4.1, for both high-Ri and low-Ri cases, as well as different downstream locations.

The fitting yielded two coefficients: α_0=1.57 and α_1=-0.46, where the higher order terms were neglected. Thus, the turbulent Schmidt number can be dynamically expressed as:

$$Sc_t = 1.57 - 0.46t \tag{4.8}$$

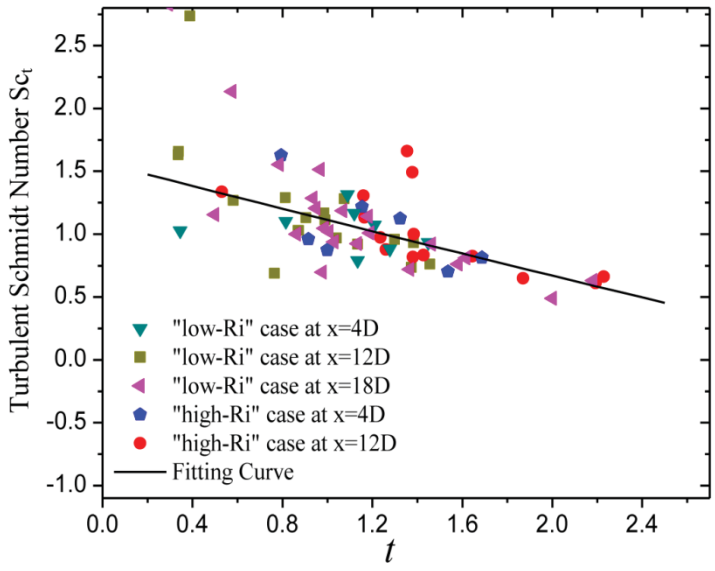

Figure 4.1. Fitting curve of Equation (4.7).

In the present study, this dynamic turbulent Schmidt number model (DTSN-Model) is applied when the velocity gradient and scalar gradient fall into the following range: $|\partial(\overline{u}_1/U_0)/\partial(x_3/D)| > 0.005$, the region where most mixing processes happened and where the experimental Sc_t values were selected for DTSN-model development. The model was implemented into the RANS models through a user-defined function.

4.3 Scalar Distribution Predictions under Various Turbulent Schmidt Numbers and Dynamic Turbulent Schmidt Number (DTSN)

Section 4.2 introduced a new dynamic turbulent Schmidt number model. By applying it to the SST $k-\omega$ model that gave the best prediction of the mean flow characteristics above, this investigation could evaluate the impact of the turbulent Schmidt number in predicting a scalar, dimensionless density difference $\theta=(\rho-\rho_{ambient})/\Delta\rho$. The "standard" turbulent Schmidt number has been controversial (He et al. 1999; Tominaga and Stathopoulos 2007). He et al. (1999) suggested $Sc_t=0.2$ for a jet-in-cross flow, which is very similar to the stratified jet in this study. A constant turbulent Schmidt number 0.7 is always recommended in commercial CFD software as the default value. The present investigation evaluates the difference in choosing three turbulent Schmidt numbers: $Sc_t=0.2$, $Sc_t=0.7$, and Sc_t determined by DTSN which is expressed in Equation (4.8).

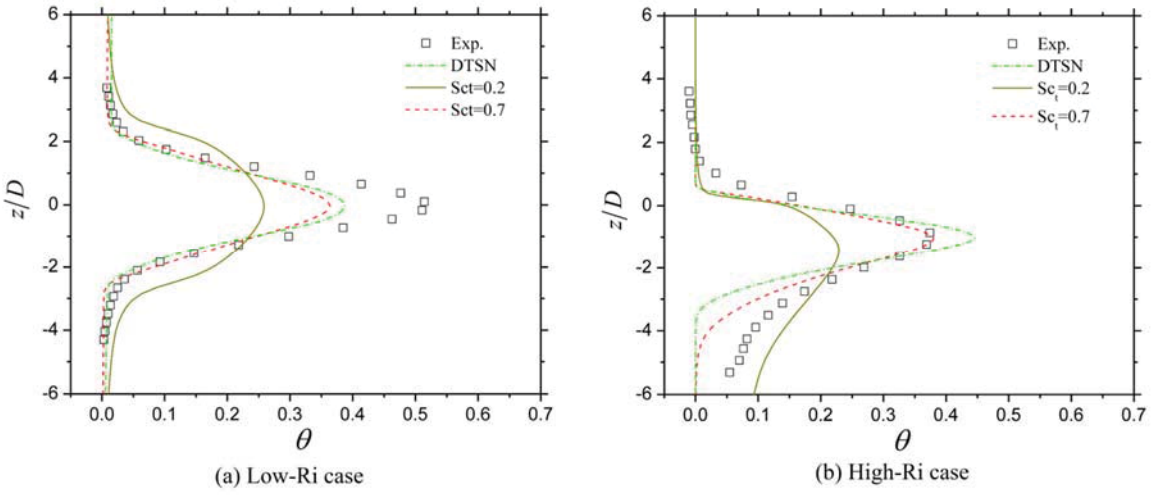

Figure 4.2. The normalized density distributions at upstream.

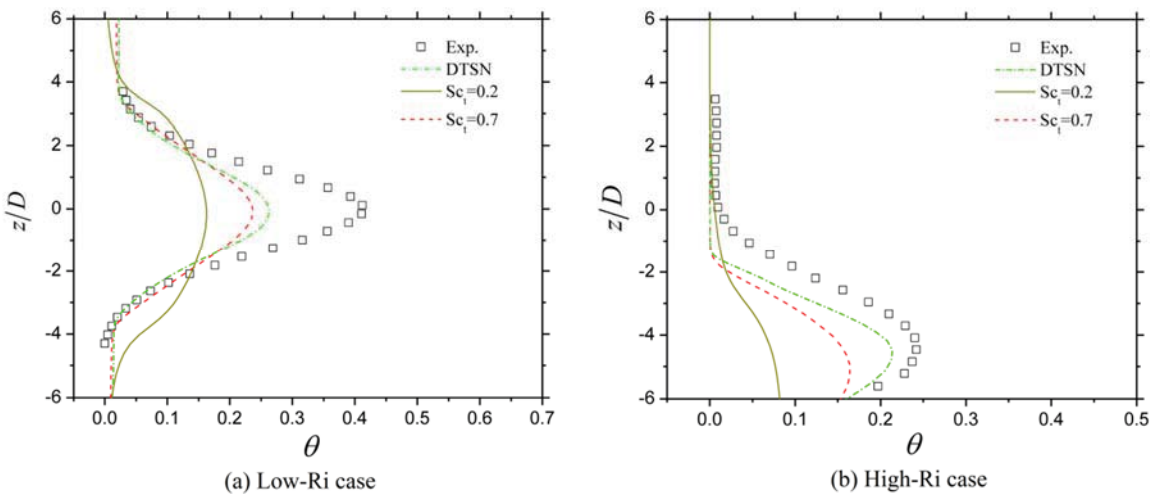

Figure 4.3. The normalized density distributions at downstream.

Fig. 4.2 and Fig. 4.3 show normalized density distributions at two different locations (between x=10D and x=20D, indicated by “upstream” and “downstream,” respectively) in both the low-Ri and high-Ri cases. The predicted density difference distributions in the stratified flows were highly dependent on the turbulent Schmidt number. The variable DTSN-model gave the best density distributions, especially in downstreams. One may also note that the larger the value of Sc_t was, the higher the predicted peak density was. This is because the mixing of the two species in the stratified flows was inversely dependent on Sc_t. A lower Sc_t can diffuse dense fluid faster into the ambient light fluid, and thus, lead to a lower peak density.

4.4 Discussion on the Additional Computational Cost

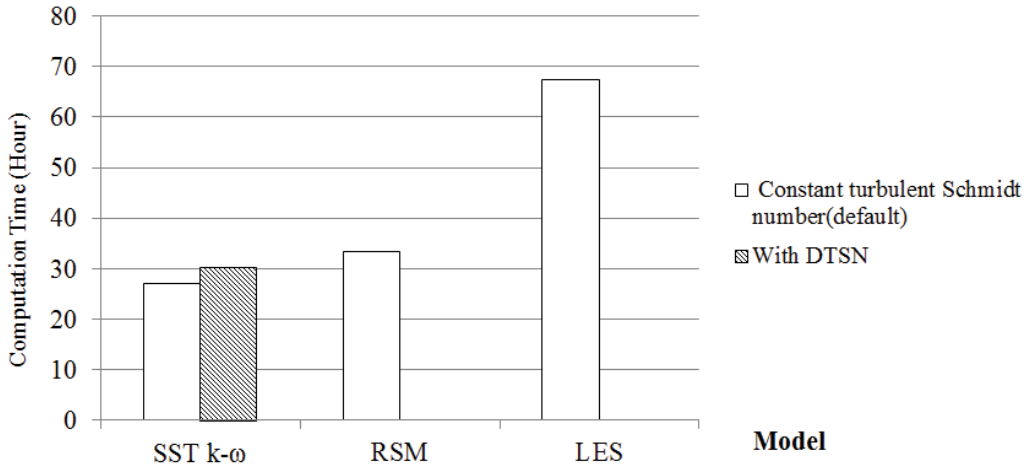

Figure 4.4. Computation times with different models.

Figure 4.4 demonstrated the comparison of computation time when a constant turbulent Schmidt number and DTSN were used. The specification of computation platform and the way computation time was estimated were exactly the same as described in section 3.6. The computation times with RSM and LES were also listed for comparison. The chart indicates that the use of DTSN requires 10% additional computation time for calculating the dynamic Schmidt number. It is also noted that even when DTSN is combined with SST $k-\omega$, the computation time is still shorter than using RSM and much shorter than using LES, when RSM and LES are using constant turbulent Schmidt numbers.

4.5 Conclusion

In this chapter, the definition of Schmidt number and turbulent Schmidt number was illustrated. It was also presented how the turbulent Schmidt number model was developed

step by step through utilizing $\overline{u_1'u_3'}$, $\overline{\theta'u_3'}$, $\frac{\partial \overline{u}_1}{\partial x_3}$ and $\frac{\partial \overline{\theta}}{\partial x_3}$ values from the dataset of Xu and Chen (2012). The result shows that density distribution in turbulent stratified flow was pretty sensitive to turbulent Schmidt number. The developed TSNM predicted good density distribution in stratified jet flows, especially at downstream locations. Moreover, the use of DTSN requires 10% additional computation time for calculating the dynamic Schmidt number, compared to using constant turbulent Schmidt number.

CHAPTER 5. GASPER-INDUCED JET FLOW SIMULATION AND AIR QUALITY ASSESSMENT

This investigation developed a CFD model to simulate gasper-induced jet flow by including detailed gasper geometry, and validated the simulation results using experimental data. A suitable turbulence model was picked up based on the findings on Chapter 3. Comparative study was done on gasper-induced flow under different initial velocities and gasper geometries. Moreover, with the validated CFD model, air quality improvement effect on passenger's breathing zone was assessed. This section reports the corresponding research results.

5.1 CFD Simulation Model

Figure 5.1 shows the geometry of a gasper in the cockpit of an MD-82 commercial airliner (Dai et al. 2014). When gasper is switched on, air is discharged from the annular outlet (red part in Fig. 5.1b), inside which there is a cone. And when a passenger tries to turn off the gasper by tuning the switch, the cone moves outward until the annular outlet is completed closed.

In this study, CFD simulation was used to investigate the air flow discharged from gasper. Experimental results from Dai et al. (2014) were used for model validation. In the experiment, gasper-induced jet flow was discharged to open air, and hotwire anemometer was used to measure the velocity at various downstream locations (Fig. 5.2). In the

simulation, a gasper 3D model with the same dimensions as the real gasper was built (Figure 5.3), and was put into a cylinder domain with diameter being 500mm and length being 600mm. Tests were done to make sure that this domain was large enough to simulate the gasper jet flow discharged into open air (further extensions of the domain did not bring much difference in simulation results). It was assumed that the flow was isothermal in simulation, since the experiment did not take temperature variation into consideration. Due to its symmetric geometry, one quarter of the air flow domain mentioned above was used for simulation, as shown in Fig. 5.4.

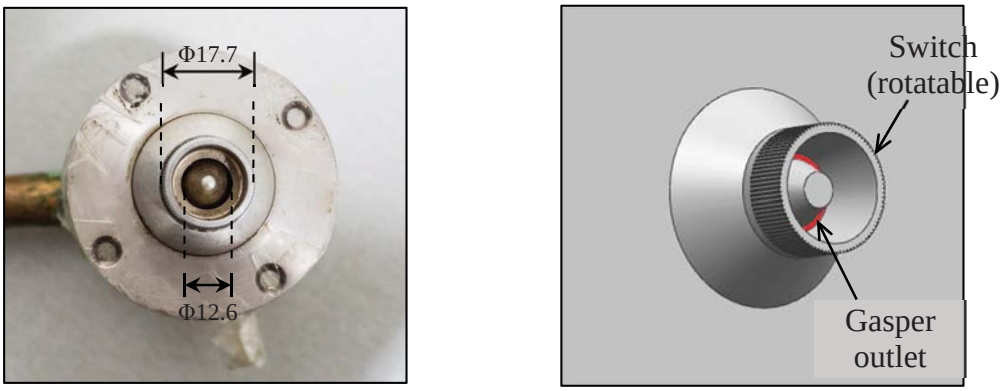

(a) A real gasper (unit: mm) (Dai et al. 2014)

(b) The CAD model with a gasper geometry

Figure 5.1. The geometry of a gasper.

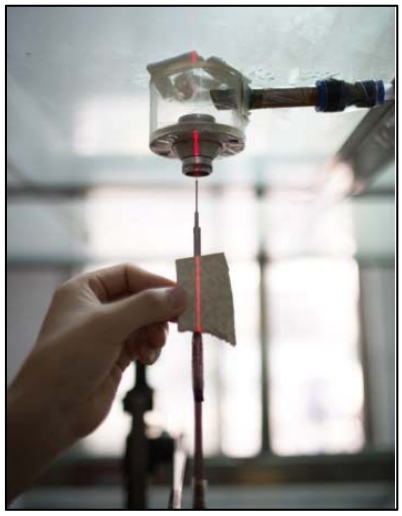

Figure 5.2. Experiment of gasper-induced jet (Dai et al. 2014).

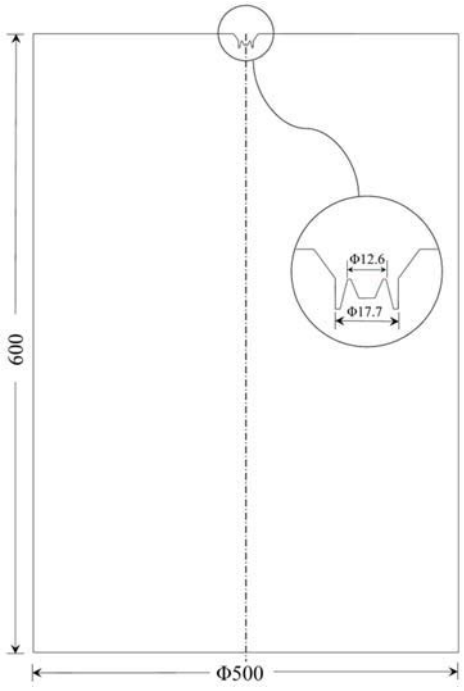

Figure 5.3. Simulation domain (unit: mm).

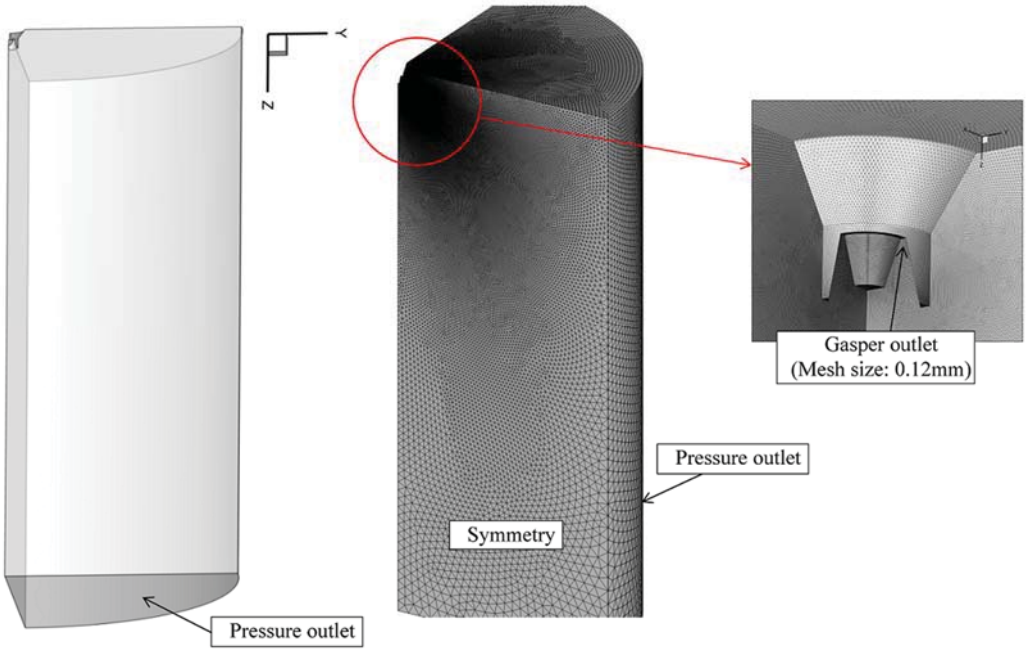

Figure 5.4. Boundary conditions and mesh structure around gasper outlet.

5.2 Simulation Method

This study used non-uniform grid size for generating the mesh in the CFD model. The mesh size was smallest around gasper nozzle and became greater as distance from nozzle was larger. Grid independence test was done, and the velocity profile along the jet axis was checked. As shown in Fig. 5.5, there was large difference between the results from "coarse" case and "medium" case, but the discrepancy between "medium" and "fine" is very minor. Thus the mesh in "medium" case was adopted for further investigation. The final number of grids was 1,445,920, and mesh size around gasper outlet region is 0.12 mm.

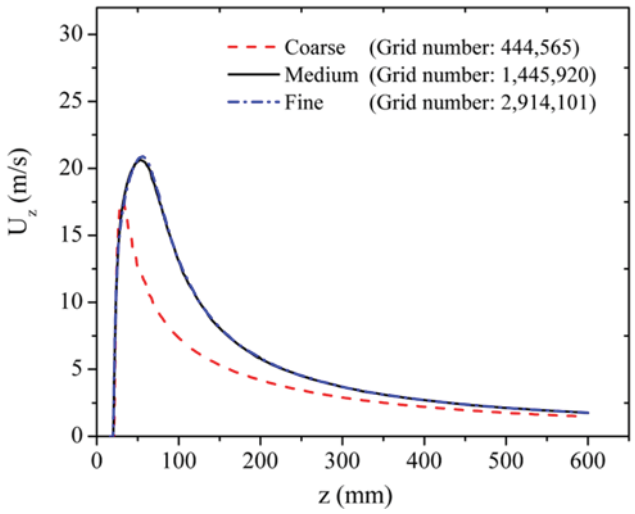

Figure 5.5. Grid independence test of gasper induced jet flow simulation.

For the boundary conditions, velocity inlet was defined for the gasper outlet. The side and bottom faces of the 1/4 cylindrical domain were defined as pressure-outlet, and standard atmospheric pressure was prescribed. Symmetry (zero-shear) boundary was used for the two symmetric faces. All other boundaries are defined as no-slip boundaries.

This investigation adopted ANSYS-Fluent 14.0 to solve for the flow field. The basic equations are continuity equation and momentum equations, which are Equation (3.1) and Equation (3.2). SIMPLE scheme was used for pressure-velocity coupling. Second order upwind discretization method was used for momentum, turbulent kinetic energy and specific dissipation rate discretization. Second order method was adopted for pressure discretization. Previous chapters showed that SST $k-\omega$ model performed better than other commonly used turbulence models in round jet simulations. Therefore, our study adopted SST $k-\omega$ model to close the RANS (Reynolds Averaged Navier-Stokes) equations. ANSYS-Fluent 14.0 solved these equations by iterations. By the end of the a calculation, residual of continuity dropped to the order of 10^{-8}, velocity residuals dropped to 10^{-7}, residual of k dropped to 10^{-6}, and residual of ω dropped to the order of 10^{-5}. Further iterations did not show much difference in the simulation results.

5.3 Results

Fig. 5.6 shows the velocity profiles of simulation results at different downstream locations. The velocity profile starts with double peaks, which were caused by the annular gasper outlet. The two peaks gradually merge to one peak as the flow goes into downstream. Fig. 5.7 shows velocity along jet axis (z direction) from simulation results, compared with experimental data (Dai et al. 2014). In this figure, z_{peak} is defined as the z location of the peak velocity along the jet axis. The comparison shows that that the simulation results match pretty well with experimental data.

On the other hand, self-similarity test was done on one-peak velocity profiles on downstream locations. Details of self-similar characteristic can be found in Pope (2000), and this characteristic was reported to be observed in turbulent round jets. In this test, $U_z/U_c - x/x_{1/2}$ curves were plotted on the same figure, where U_c is defined as the z-velocity on centerline, and $x/x_{1/2}$ was defined as the x location at which z-velocity is half of U_c. Figure 5.8 shows the curves at 3 downstream locations. The 3 curves collapse into almost a single one after normalization, which shows the self-similarity of the velocity profiles. This further demonstrates the validity of the above CFD model in simulating gasper-induced jet flows.

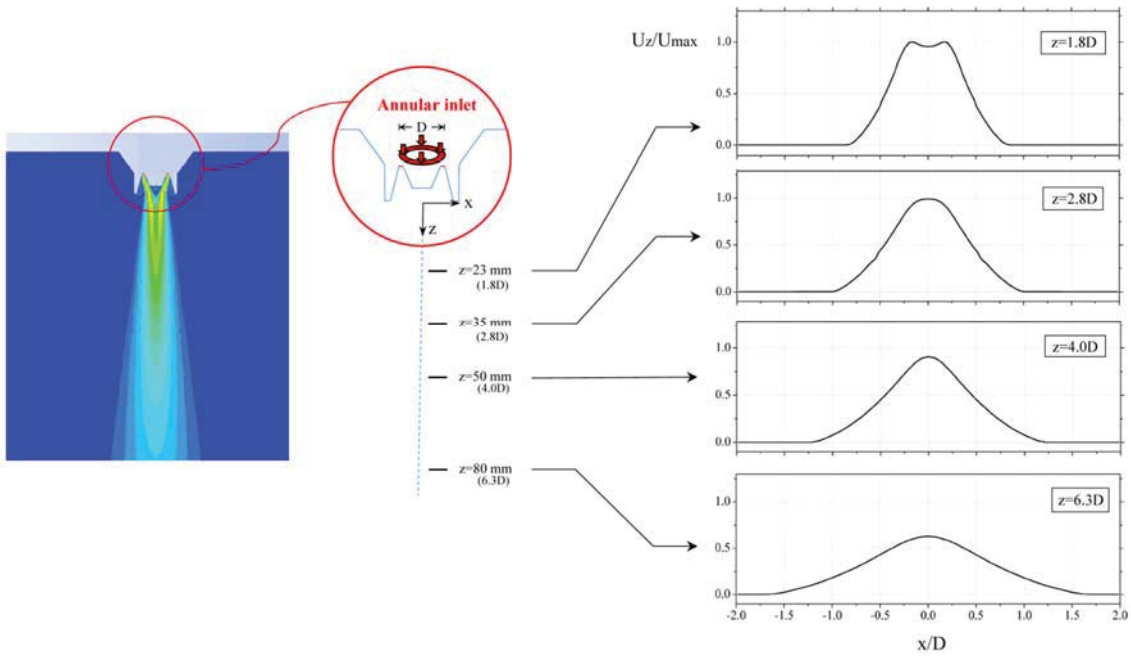

Figure 5.6. Lateral velocity profile development along jet axis.

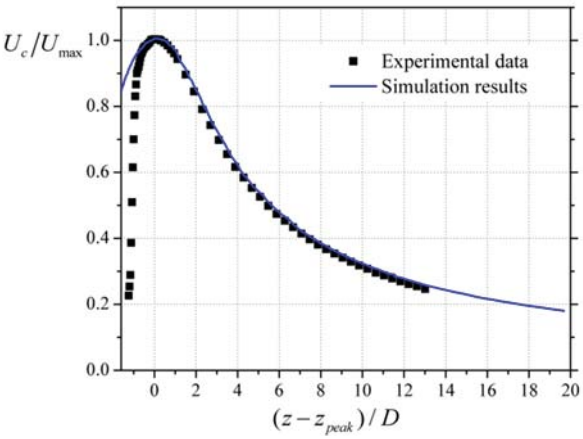

Figure 5.7. Centerline velocity from simulation results and experimental data from Dai et al. (2014).

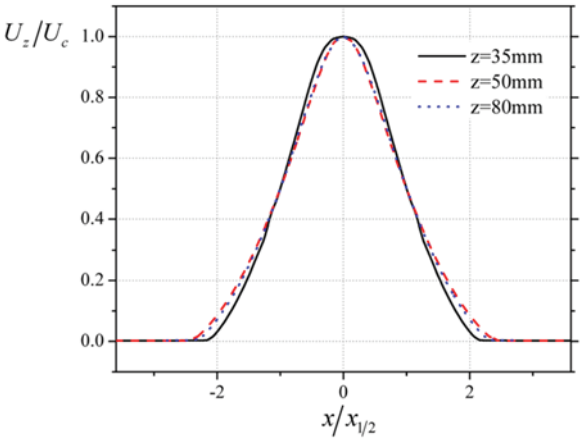

Figure 5.8. Self-similarity curves.

With the validated CFD model, we further explored more flow characteristics of gasper-induced flow, and how the flow pattern changes with the change of initial velocities and gasper geometries.

Figure 5.9 shows streamlines and velocity contours of gasper-induced jet flow close to gasper outlet region. Although only one quarter of the fluid domain was simulated in CFD model, the other half of the results were mirrored in Fig. 5.9 along the jet axis, so that a more realistic flow feature could be demonstrated. It was observed that due to Coanda effect (Wille and Fernholz 1965), air from gasper annular outlet immediately attaches to the cone wall inside the annular outlet. Further downstream, the flow around cone merges into a single stream, and the merging point is where velocity profiles change from "two-peak" curve to "one-peak". This also generates vortices in the flow. Meanwhile, on this cross section view of the streamlines, z-stagnation points were defined where the z-velocity of the flow started to change from negative value to a

positive one. This is also the point where the ambient flow is “formally” entrained into the jet mainstream. The z-stagnation points form a z-stagnation line at each side of the jet on this cross-section.

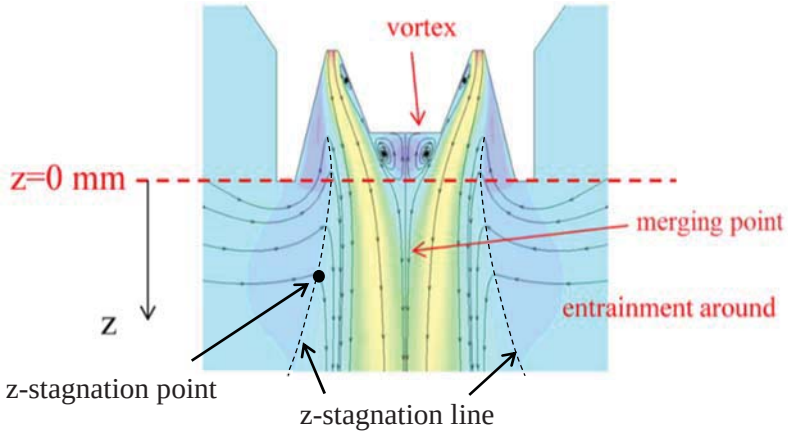

Figure 5.9. Streamlines near gasper outlet region.

This section also discusses gasper-induced flows under different initial gasper outlet velocities (case 1, 2 and 3) and gasper geometries (case 1 and 4), as listed in Table 5.1. Velocity profiles at jet center axis were examined, since it indicates how jet develops and decays after discharged from the annular outlet.

Table 5.1. Specifications of cases 1-4.

Case #	Initial velocity at gasper outlet	Gasper outlet location
1	40	Original location
2	60	Original location
3	80	Original location
4	40	Moved outward by 37.5 mm

5.3.1 Different Gasper Outlet Velocity

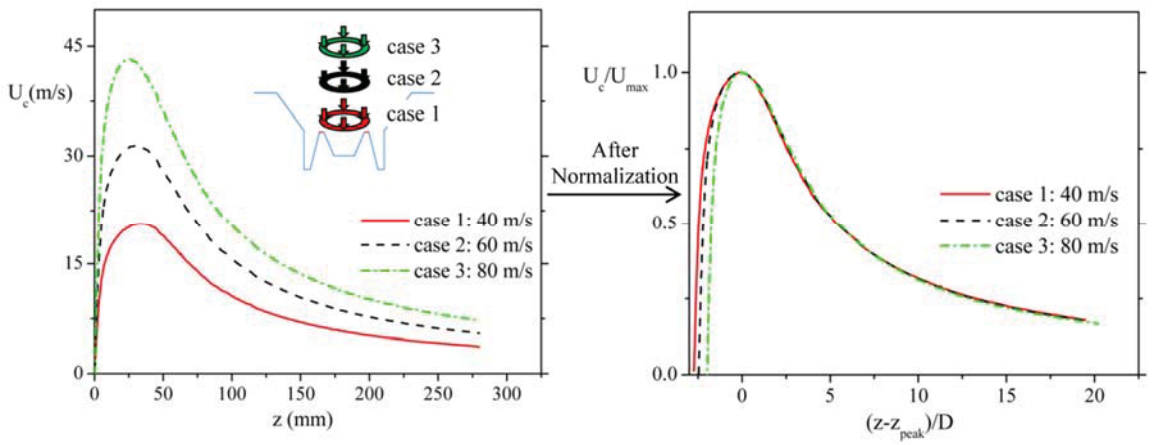

(a) Before normalization (b) After normalization

Figure 5.10. Centerline velocity profiles under different initial velocities.

When gaspers are on, the initial velocities of gasper-induced jets can be different, depending on the air pressures inside gaspers. Figure 5.10a demonstrates 3 centerline velocity profiles under 3 different initial velocities. With different initial velocities, the profiles of centerline velocities are very similar. When normalized by maximum centerline velocities and gasper outlet diameter, these profiles collapse into almost a single curve. This phenomenon is more obvious at locations after the peak locations, where the velocities are decaying along central axes.

5.3.2 Different Gasper Outlet Depths

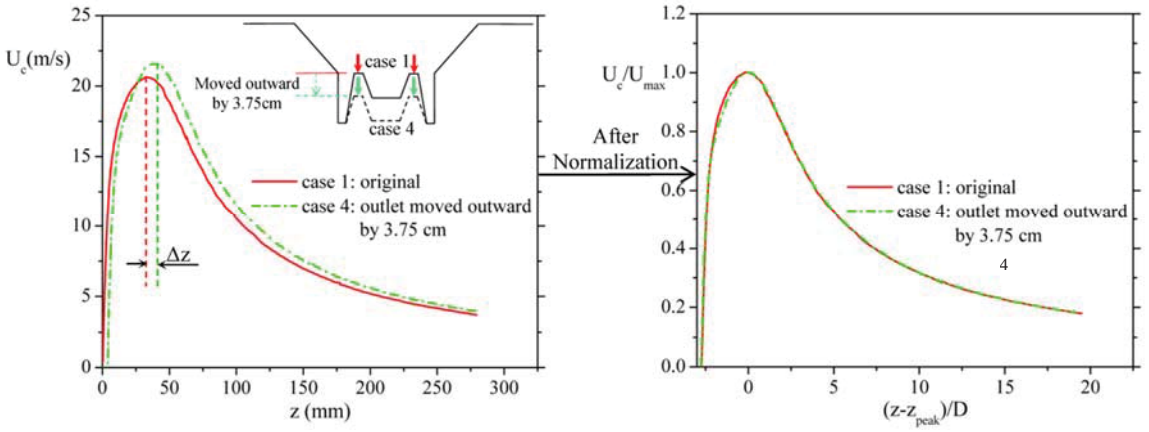

(a) Before normalization (b) After normalization

Figure 5.11. Centerline velocity profiles under different gasper outlet depth.

When a passenger adjusts a gasper, the "cone" structure inside is rotated to move inward or outward. As a result, gasper outlet can be at different depths. Figure 5.11 (a) shows centerline velocity profiles of gasper-induced jet flows when gasper outlet is at 2 different depths. Basically after the gasper outlet is moved outward, the centerline velocity profile offsets outward by a certain distance as well. When normalized, the two curves collapse into almost a single curve, which is similar as what is observed in jet centerline velocity profiles under various initial velocities.

5.4 Velocity Profile Modeling of Gasper-induced Jets

Section 5.3 above demonstrated the phenomenon that all gasper centerline velocity profiles collapse into a single curve after normalized by gasper outlet diameter and maximum centerline velocity, regardless of gasper outlet initial velocity and gasper

geometry (outlet depth of cone). Based on this observation, this paper further developed a gasper centerline velocity model (GCVM) for gasper-induced jet flow centerline velocity prediction. The model is written as

$$\frac{U_c}{U_{\max}} = g(\delta) = \begin{cases} 1.49\delta^3 + 2.31\delta^2 + 1.19\delta + 1.18, z < z_{peak} \\ \dfrac{0.42\delta + 1}{0.12\delta^2 + 0.37\delta + 1}, z > z_{peak} \end{cases} \tag{5.1}$$

where $\delta = (z - z_{peak}) / D$.

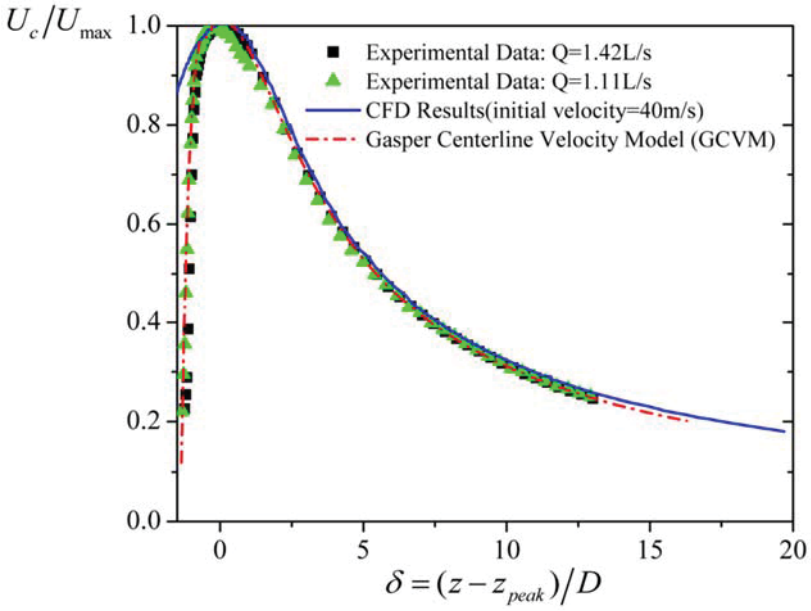

Figure 5.12. Comparison of GCVM result, experimental data and CFD result.

Fig. 5.12 illustrates the centerline velocity predicted by GCVM, experimental results (Dai et al. 2014) under two flow rates, and velocity profile from one CFD model. The result shows that the proposed velocity model can predict centerline velocity development in gasper-induced jet pretty well.

On the other hand, at downstream locations of gasper induced jet, the lateral velocity profiles follow self-similarity characteristics, as indicated in section 5.3. This study also developed a gasper downstream lateral velocity model (GDLV) to calculate the lateral z-velocity (normalized by centerline velocity) through lateral locations (normalized by $x_{1/2}$) at downstream.

$$\frac{U_z}{U_c} = e^{-\frac{5}{8}\chi^2}, \tag{5.2}$$

where $\chi = x/x_{1/2}$.

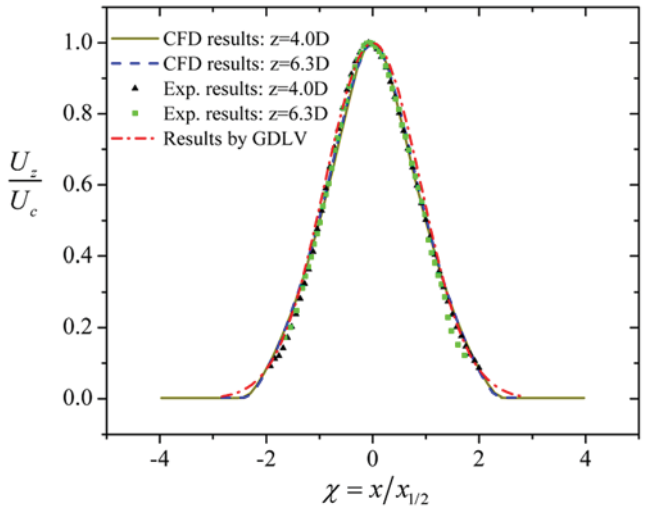

Figure 5.13. Comparison of GDLV result, experimental data (Dai et al. 2014) and CFD result.

Figure 5.13 illustrates the comparison of normalized velocities calculated by GDLV, measured by experiments (Dai et al. 2014), and predicted by CFD model. The GDLV results were in good match with experimental results and CFD results.

In GDLV model, $\frac{U_z}{U_c}$ is calculated through the parameter χ, which is the lateral location (X) normalized by half velocity location $x_{1/2}$. With the validated CFD model, this paper was able to investigate how $x_{1/2}$ developed along the jet axis. As illustrated in Fig. 5.14, at the vicinity of gasper outlet, $x_{1/2}/D$ increased quadratically along axis; however, at further downstream there was a strong linear relationship between $x_{1/2}/D$ and δ.

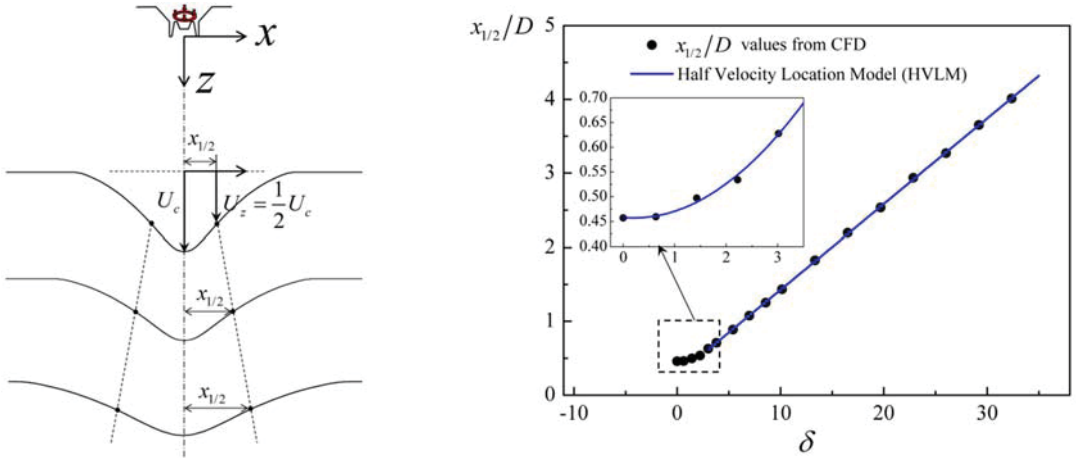

(a) Sketch of lateral velocity profile at different downstream locations

(b) Relationship between $x_{1/2}/D$ and δ

Figure 5.14. Development of $x_{1/2}$ along jet axis.

Based on these observations, this paper proposed a half velocity location model (HVLM) to characterize the $x_{1/2}/D$ profile along jet axis:

$$\frac{x_{1/2}}{D} = h(\delta) = \begin{cases} 0.021\delta^2 - 0.0087\delta + 0.478, & \delta \le 3 \\ 0.116\delta + 0.270, & \delta > 3 \end{cases} \tag{5.3}$$

This model could be used to support GDLV model, so that $x_{1/2}$ could be calculated based on jet axis location.

The two models (GCVM and GDLV) described above, when combined, can not only be useful in predicting velocities at different downstream locations on gasper-induced jet centerlines without doing experiments or CFD simulations, but also provide good information in design or analysis of gasper or nozzles with similar geometry.

5.5 Gasper-induced Jet Flow Rate Modeling

The modeling of centerline velocity profile and lateral velocity profile in gasper-induced jet flow enables the derivation of U_z in the whole flow domain, and thus the mathematical modeling of flow rate at any given jet downstream location.

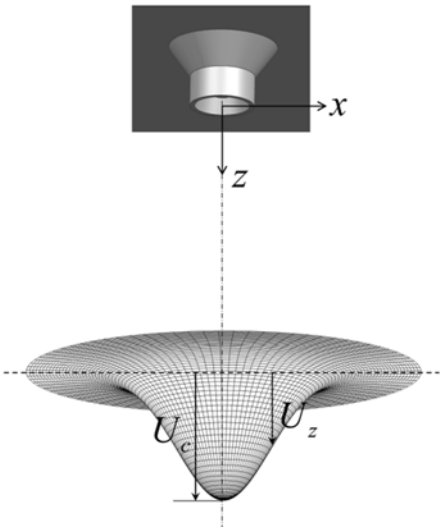

Figure 5.15. Z-direction velocity profile at a gasper induced jet flow downstream location.

Figure 5.15 demonstrated a schematic profile of U_z at a downstream location. Integrating U_z on the whole cross-section area by combining GCVM and GDLV models yields

$$Q = \iint U_z dA = \int_0^\infty U_z \cdot 2\pi x dx = \int_0^\infty e^{-\frac{5}{8}\chi^2} U_c \cdot 2\pi x dx = \int_0^\infty e^{-\frac{5}{8}\left(\frac{x}{x_{1/2}}\right)^2} U_c \cdot 2\pi x dx$$

$$= \int_0^\infty e^{-\frac{5}{8}\left(\frac{x}{h(\delta)D}\right)^2} g(\delta) U_{\max} \cdot 2\pi x dx \qquad (5.4)$$

Where $g(\delta) = \begin{cases} 1.49\delta^3 + 2.31\delta^2 + 1.19\delta + 1.18, z < z_{peak} \\ \dfrac{0.42\delta + 1}{0.12\delta^2 + 0.37\delta + 1}, z > z_{peak} \end{cases}$, and

$$h(\delta) = \begin{cases} 0.021\delta^2 - 0.0087\delta + 0.478, & \delta \le 3 \\ 0.116\delta + 0.270, & \delta > 3 \end{cases}$$

One may note that in Equation (5.4), it is not possible to express the integral in a symbolic function. However, it is still possible to calculate the definite integral by using Newton-Cotes formulae (Abramowitz and Ategun 1972) as follows.

$$Q = \int_0^\infty e^{-\frac{5}{8}\left(\frac{x}{h(\delta)D}\right)^2} g(\delta) U_{\max} \cdot 2\pi x dx = \sum_{i=1}^{n} e^{-\frac{5}{8}\left(\frac{x_i}{h(\delta)D}\right)^2} g(\delta) U_{\max} \cdot 2\pi x_i \Delta x \qquad (5.5)$$

where $x_{i+1} = x_i + \Delta x$, and n is determined when the value of $e^{-\frac{5}{8}\left(\frac{x_{n+1}}{h(\delta)D}\right)^2} g(\delta) U_{\max} \cdot 2\pi x_{n+1}$ is negligible. MATLAB can be used to calculate the sum in Equation (5.5).

5.6 Air Quality Improvement Effect Assessment on Gasper

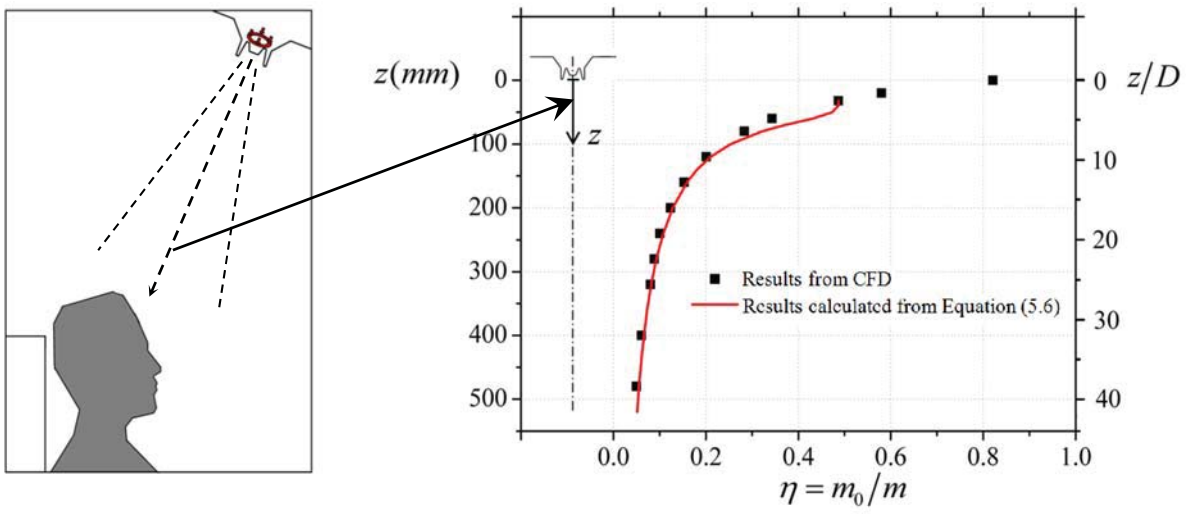

Figure 5.16. Fresh air ratio along jet axis.

Both the proposed flow rate model and validated CFD model and were used for analyzing entrainment effect due to gasper-induced jet flow in this current research. To quantify this effect, entrainment ratio ε is defined. This ratio is calculated as $\varepsilon = \frac{\dot{m}}{\dot{m}_0}$, where $\dot{m}_0$ is the mass flow rate at jet nozzle, and $\dot{m}$ is the mass flow rate at a certain downstream of jet mainstream. The ratio was used by a lot of previous literatures, such as Ricou and Spalding (1961). In current study, fresh air fraction is further defined as $\eta = \frac{1}{\varepsilon} = \frac{\dot{m}_0}{\dot{m}}$, to quantify the air quality, since it indicates the percentage of fresh air (the air that is discharged from gasper nozzle) at a downstream jet location. Thus the greater the fresh air fraction is, the higher the air quality is.

In CFD method, $\dot{m}$ was calculated by reporting the flow rate at different downstream locations inside the envelope formed by z-stagnation lines, which was mentioned in Section 5.3.

On the other hand, in analytical method (the method with flow rate model), η was calculated as

$$\eta = \frac{m_0}{m} = \frac{m_0/\rho}{m/\rho} = \frac{Q_0}{Q}$$

By using gasper induced jet flow rate model,

$$\frac{Q}{Q(\delta=0)} = \frac{\int_0^\infty e^{-\frac{5}{8}\left(\frac{x}{h(\delta)D}\right)^2} g(\delta) U_{\max} \cdot 2\pi x dx}{\int_0^\infty e^{-\frac{5}{8}\left(\frac{x}{h(0)D}\right)^2} g(0) U_{\max} \cdot 2\pi x dx}$$

It was obtained from section 4.3 that $g(0)=1$ and $h(0)=0.478$. Thus $\frac{Q}{Q(\delta=0)}$ can be simplified as

$$\frac{Q}{Q(\delta=0)} = \frac{\int_0^\infty e^{-\frac{5}{8}\left(\frac{x}{h(\delta)D}\right)^2} g(\delta) x dx}{\int_0^\infty e^{-\frac{5}{8}\left(\frac{x}{0.478D}\right)^2} x dx} \tag{5.6}$$

Fig. 5.16 illustrates the development of fresh air fraction v.s. axial distance, from both methods. Results demonstrated that the fresh air fractions predicted by CFD and that

calculated analytically were pretty close, especially at jet downstream locations. The minor discrepancy between the two results near $\delta = 0$ could be because jet did not fully develop close to gasper outlet, where $U_z/U_c - x/x_{1/2}$ relationship did not fully become self-preserving. Thus GDLV model was not able to accurately define the lateral velocity distribution at that region.

Both results showed that fresh air fraction dropped dramatically as distance from jet nozzle increases. In the aircraft cabin mockup from Anderson (2012), he used 0.48m (480mm) as the minimum vertical distance from a human simulator's inhalation zone to gasper nozzle. In Fig. 5.16, the CFD results show fresh air fraction is about 5% at location z=480 mm. In other words, even when gasper is turned on, about 5% of the air in breathing zone is fresh air, while more than 90% of air comes from ambient. This result shows that the effect of air quality improvement in passenger's breathing zone by gasper may be very minor. By taking into consideration that in real situation turning on the gasper may decrease the air flow rate from main ventilation system, which means less dilution of contaminant in the cabin, it is even possible that the gasper-induced jet flow actually decreases the air quality level in the passenger's breathing zone. The results also demonstrated the validity of gasper induced jet flow rate model in predicting flow rate and entrainment ration in gasper jet flows.

5.7 Conclusion

In this chapter, CFD simulations of gasper-induced jet flow with detailed gasper geometry were described. SST $k-\omega$ model, which was proved to be one of the best turbulence models in jet simulation, was selected for closing the RANS equations. The simulation results were further validated by experimental results with the same gasper geometry. The results were showing that SST $k-\omega$ model can give good prediction of gasper-induced jet flows. The simulation captured the velocity profiles on the transverse direction which started from “double-peak” curve, and transited to “single-peak” curve after the merging point. In addition, it was shown that the axial velocity profiles under different initial velocities and gasper geometries show self-similarity characteristics, by examining the normalized centerline velocity profiles. Three models were developed to calculate gasper-induced jet centerline velocities, lateral velocities, and flow rates at different downstream locations. Moreover, through investigating the fresh air ratio at different downstream locations of the gasper-induced jet, this study found more than 90% of the air in the breathing zone was from the ambient environment. The gasper-induced jet flow may only have very minor effect on decontaminating the air in a passenger’s breathing zone, or may even lower its the air quality if the main ventilation flow rate is taken into consideration.

CHAPTER 6. CONCLUSIONS AND FUTURE WORKS

This chapter summarizes the major conclusions in this research. Meanwhile, potential research topics based on current investigation are also indicated.

6.1 Conclusions

This study used MSE to quantitatively assess the performances of six RANS models and one LES model in the simulation of stratified flows. Both first order flow characteristics (mean velocity and mean density) and second order momentums (TKE and turbulent shear stress) were examined in the evaluation. The results showed that in weakly stratified jet, all seven models predicted the mean velocity with good accuracy, but the predictions of TKE and turbulent shear stress were quite different with different models. RNG $k-\varepsilon$ and SST $k-\omega$ yielded pretty good overall results in Low-Ri case, and SST $k-\omega$ was the best. It was also observed that adopting LES did not give better predicting results than using RANS model in terms of TKE and turbulent shear stress simulation results. In strongly stratified jet, on the other hand, the prediction results were not as good as in weakly stratified case. For mean velocity, most of the turbulence models still gave good predictions of the mean flow, except LES and RSM models, which overestimated the mean velocity in unstable stratified region. In terms of second-order flow

characteristics, RSM, SST $k-\omega$, and RNG $k-\varepsilon$ yielded better results that other models. Among them, RSM and SST $k-\omega$ models were the best. In high-Ri case, it was shown again that LES does not always predict better results than RANS models. One of the reasons is might be that LES with the standard Smagorinsky model may not be suitable for the low Reynolds number transitional flows in the strongly stratified flow.

In current study, by using different turbulent Schmidt numbers in predicting density distributions, we found that the scalar (density) distribution in stratified flows is very sensitive to turbulent Schmidt number, which agreed with the finding in a lot of previous literatures. The study developed a new DTSN model, which calculates the local turbulent Schmidt number through the local velocity gradient and density gradient. The model was developed based on the experimental dataset from Xu and Chen (2012). Results showed that the proposed model could improve density field distribution, especially at the downstream locations at a jet.

This investigation further compared the computational costs by the simulations using different turbulence models. The tests were done tested using one node of a Linux-cluster with two 2.5 GHz Quad-Core AMD 2380 processors. Results indicated that computation time with five eddy-viscosity models ($k-\varepsilon$ models and $k-\omega$ models) were comparable. However, RSM, which is a seven equation model, required 25% more computing time compared with eddy-viscosity models. And LES needed almost three times computation time as simulation with eddy-viscosity models. The study also found that the adoption of DTSN required 10% additional computing time in the simulation with the same turbulence model.

The developed CFD models for stratified jets predicted vorticity distribution in both low-Ri and high-Ri cases with reasonable accuracy. The CFD models were also used for investigating the entrainments in stratified jets. Results showed that the empirical formula could be used for calculating the entrainment ratio in weakly stratified jet but not in strongly stratified one.

Moreover, this investigation built a CFD model to simulate gasper-induced jet flows with detailed gasper geometry. The selected turbulence model was SST $k-\omega$ model, which was shown to be one of the best turbulence models in simulating jet flows under both high turbulence and low turbulence levels in this study. The simulation results were validated by experimental data. The results indicated that the centerline velocity profiles under different velocities and gasper geometries collapsed into a single curve after normalization, which could be described by a proposed mathematical model. A lateral velocity model was also proposed to predict the lateral velocity distributions at gasper-induced jet flow downstream locations. These two models further enabled the establishment of a flow rate model in such flows. The proposed flow rate model and CFD model were used together to assess the air quality in passenger's breathing zone. Less than 10% of the air in the breathing zone was the fresh air from the gasper. Turning on gasper may have very limited effect on improving air quality, or may even damage the air quality in breathing zone.

6.2 Future Works

Although this investigation studied stratified jet flows and gasper-induced jet flow using numerical simulations, which led to some conclusions, there are several aspects where the current work can be improved, or future research can be conducted.

First, the experimental dataset that current study used for evaluating model performances was from an experiment in which round jets were discharged into light fluid tank. Thus in the CFD simulation, the same fluid domain was used. Future researches on stratified jet flows can expand the simulations to a larger indoor environment, such as an office or an aircraft cabin, where impingement, thermal plume, or cross-flows may exist. Such simulations will be more complicated yet can simulate stratified jets in indoor environments in a more realistic way.

Second, regarding gasper-induced jet flow, this study developed a mathematical model to calculate the normalized velocity profiles for such flow. However, more work is needed as to how to calculate the peak velocity and peak velocity location based on gasper geometry and initial conditions. With that being done, the current mathematical model can be improved into a more useful model, which can be generally applied.

Third, the study on gasper-induced jet flow in current investigation mainly focused on the local flow features adjacent to the gasper nozzle. Future works can also expand the study to a full aircraft cabin to discover the interplay of gasper-induced jet with other forms of flows. It is also interesting to carry out experimental researches to validate the corresponding simulation results.

LIST OF REFERENCES

LIST OF REFERENCES

Abramowitz, M., and Stegun, I. A. (Eds.). 1964. *Handbook of mathematical functions: with formulas, graphs, and mathematical tables* (No. 55). Mineola, NY: Courier Corporation.

Air Transport Medicine Committee. 1997. "The Very Large Airplane: Safety, Health and Comfort Considerations." *Aviation, Space and Environmental Medicine* 68(10).

Anderson, M. D. 2012. "Effect of gaspers on airflow patterns and the transmission of airborne contaminants within an aircraft cabin environment." *Dissertation Kansas State University*.

ANSYS Inc. 2011. ANSYS Fluent Theory Guide, release 14.0 [online]. Available from http://www.ansys.com [Accessed November 2012]

Armenio, V., and Sarkar, S. 2002. "An investigation of stably stratified turbulent channel flow using large-eddy simulation. " *Journal of Fluid Mechanics* 459: 1-42.

Bacon, S. 1998. "Decadal variability in the outflow from the Nordic seas to the deep Atlantic Ocean." Nature 394(6696): 871-874.

Baker, O. 1953. "Design of pipelines for the simultaneous flow of oil and gas." *In Fall Meeting of the Petroleum Branch of AIME. Society of Petroleum Engineers*.

Blocken, B., Stathopoulos, T., and Carmeliet, J. 2007. "CFD simulation of the atmospheric boundary layer: wall function problems." *Atmospheric environment* 41(2):238-252.

Britter, R., and Schatzmann., M. (Ed.). 2007. "Background and justification document to support the model evaluation guidance and protocol: COST action 732 Quality assurance and improvement of microscale meteorological models." Hamburg: University of Hamburg Meteorological Institute.

Brown, T. P., Shuker, L. K., Rushton, L., Warren, F., and Stevens, J. 2001. "The possible effects on health, comfort and safety of aircraft cabin environments." *The journal of the Royal Society for the Promotion of Health* 121(3): 177-184.

Cropper, P. C., Yang, T., Cook, M., Fiala, D., and Yousaf, R. 2010. "Coupling a model of human thermoregulation with computational fluid dynamics for predicting human–environment interaction." *Journal of Building Performance Simulation* 3(3): 233-243.

Cussler, E. L. 2009. "Diffusion: mass transfer in fluid systems." Cambridge: Cambridge university press.

Dai, S., Guo, Y., and Liu, J. 2014. "Experimental study of characteristics of aircraft gasper isothermal jet." *Proceedings of the 13th International Conference on Air Distribution in Rooms (ROOMVENT 2014),* Sao Paulo, Brazil.

Dalziel, S. B., Carr, M., Sveen, J. K., and Davies, P. A. 2007. "Simultaneous synthetic schlieren and PIV measurements for internal solitary waves." *Measurement Science and Technology* 18 (3): 533.

Davidson, L., Nielsen, P. V., and Sveningsson, A. 2003. "Modifications of the V2 Model for Computing the Flow in a 3D Wall Jet." *Modifications of the Model for Computing the Flow in a 3D Wall Jet.*

Franke, J., Bartzis, J., Barmpas, F., Berkowicz, R., Brzozowski, K., Buccolieri, R., Carissimo, B., Costa, A., Di Sabatino, S., Efthimiou, G., Goricsan, I., Hellsten, A., Ketzel, M., Leitl, B., Nuterman, R., Olesen, H., Polreich, E., Santiago, J., and Tavares, R. 2008. "The MUST model evaluation exercise: Statistical analysis of modelling results." *Hrvatski meteorološki časopis* 43(43/1): 414-418.

Gao, N. P., and Niu, J. L. 2008. "Personalized ventilation for commercial aircraft cabins." *Journal of Aircraft* 45(2): 508-512.

Ghaisas, N. S., Shetty, D. A., and Frankel., S. H. 2013. "Large eddy simulation of thermal driven cavity: Evaluation of sub-grid scale models and flow physics." *International Journal of Heat and Mass Transfer* 56(1): 606-624.

Gibson, M. M., and Launder, B. E. 1978. "Ground effects on pressure fluctuations in the atmospheric boundary layer." *Journal of Fluid Mechanics* 86(03): 491-511.

Gupta, J. K., Lin, C. H., and Chen, Q. 2010. "Characterizing exhaled airflow from breathing and talking." *Indoor Air* 20(1): 31-39.

Gupta, J.K., Lin, C.-H., and Chen, Q. 2011. "Can gaspers provide protection from airborne contaminants to the occupants in an airliner cabin?" *Proceedings of the 12th International Conference on Indoor Air Quality and Climate (Indoor Air 2011),* Austin, Texas.

Gupta, J. K., Lin, C. H., and Chen, Q. 2012. "Risk assessment of airborne infectious diseases in aircraft cabins." *Indoor Air* 22(5): 388-395.

Hansen, B., and Østerhus, S. 2000. "North Atlantic–Nordic Seas exchanges." *Progress in Oceanography* 45(2): 109-208.

He, G., Guo, Y., and Hsu, A. T. 1999. "The effect of Schmidt number on turbulent scalar mixing in a jet-in-crossflow." *International Journal of Heat and Mass Transfer* 42(20): 3727-3738.

Hill, B. J. 1972. "Measurement of local entrainment rate in the initial region of axisymmetric turbulent air jets." *Journal of Fluid Mechanics* 51(04): 773-779.

Hunt, J. C. R., and Snyder, W. H. 1980. "Experiments on stably and neutrally stratified flow over a model three-dimensional hill." *Journal of Fluid Mechanics* 96(04): 671-704.

Incropera, F. P. 2011. "Fundamentals of heat and mass transfer." Hoboken: John Wiley & Sons.

International Air Transport Association (IATA). 2013. "Airlines Expect 31% Rise in Passenger Demand by 2017." [Accessed January 2015]

Jacobitz, F. G., Sarkar, S., and van Atta, C. W. 1997. "Direct numerical simulations of the turbulence evolution in a uniformly sheared and stably stratified flow." *Journal of Fluid Mechanics* 342: 231-261.

Ji, Y., Cook, M. J., Hanby, V., Infield, D. G., Loveday, D. L., and Mei, L. 2008. "CFD modelling of naturally ventilated double-skin facades with Venetian blinds." *Journal of Building Performance Simulation* 1(3): 185-196.

Karimipanah, T., and Awbi, H. B. 2002. "Theoretical and experimental investigation of impinging jet ventilation and comparison with wall displacement ventilation." *Building and Environment* 37(12): 1329-1342.

Kenyon, T. A., Valway, S. E., Ihle, W. W., Onorato, I. M., and Castro, K. G. 1996. "Transmission of multidrug-resistant Mycobacterium tuberculosis during a long airplane flight." *New England Journal of Medicine* 334(15): 933-938.

Kneller, B. C., Bennett, S. J., and McCaffrey, W. D. 1999. "Velocity structure, turbulence and fluid stresses in experimental gravity currents." *Journal of Geophysical Research: Oceans (1978–2012)* 104 (C3): 5381-5391.

Komori, S., Ueda, H., Ogino, F., and Mizushina, T. 1983. "Turbulence structure in stably stratified open-channel flow." *Journal of Fluid Mechanics* 130(13-26): 2.

Kühn, M., Bosbach, J., and Wagner, C. 2009. "Experimental parametric study of forced and mixed convection in a passenger aircraft cabin mock-up." *Building and Environment* 44(5): 961-970.

Launder, B. E., Reece, G. J., and Rodi, W. 1975. "Progress in the development of a Reynolds-stress turbulence closure." *Journal of Fluid Mechanics* 68(03): 537-566.

Launder, B. E. 1989. "Second-moment closure: present… and future?." *International Journal of Heat and fluid flow* 10(4): 282-300.

Launder, B. E., and Spalding, D. B. 1972. "Lectures in mathematical models of turbulence." London: Academic press.

Lehmann, E. L., and Casella, G. 1998. *Theory of point estimation.*Vol. 31. Berlin: Springer.

Lienhard V, J. H., and Van Atta, C. W. 1990. "The decay of turbulence in thermally stratified flow." *Journal of Fluid Mechanics* 210: 57-112.

Lin, C. H., Wu, T. T., Horstman, R. H., Lebbin, P. A., Hosni, M. H., Jones, B. W., and Beck, B. T. 2006. "Comparison of large eddy simulation predictions with particle image velocimetry data for the airflow in a generic cabin model." *HVAC&R Research* 12(S3): 935-951.

Liu, W., Mazumdar, S., Zhang, Z., Poussou, S. B., Liu, J., Lin, C. H., and Chen, Q. 2012a. "State-of-the-art methods for studying air distributions in commercial airliner cabins." *Building and Environment* 47: 5-12.

Liu, W., Wen, J., Chao, J., Yin, W., Shen, C., Lai, D., Lin, C. H., Liu, J., Sun, H., and Chen, Q. 2012b. "Accurate and high-resolution boundary conditions and flow fields in the first-class cabin of an MD-82 commercial airliner." *Atmospheric Environment* 56: 33-44.

Liu, W., Wen, J., Lin, C. H., Liu, J., Long, Z., and Chen, Q. 2013. "Evaluation of various categories of turbulence models for predicting air distribution in an airliner cabin." *Building and Environment* 65: 118-131.

Liu, X., Niu, J., Perino, M., and Heiselberg, P. 2008. "Numerical simulation of inter-flat air cross-contamination under the condition of single-sided natural ventilation." *Journal of Building Performance Simulation* 1(2): 133-147.

Mahrt, L., Vickers, D., Nakamura, R., Soler, M. R., Sun, J., Burns, S., and Lenschow, D. H. 2001. "Shallow drainage flows." *Boundary-layer meteorology* 101(2): 243-260.

Marmur, A., and Mamane, Y. 2003. "Comparison and evaluation of several mobile-source and line-source models in Israel." *Transportation Research Part D: Transport and Environment* 8(4): 249-265.

Mazumdar, S., and Chen, Q. 2008. "Influence of cabin conditions on placement and response of contaminant detection sensors in a commercial aircraft." *Journal of Environmental Monitoring* 10(1): 71-81.

Melikov, A. K. 2004. "Personalized ventilation." *Indoor Air* 14(s7): 157-167.

Menter, F. R., Kuntz, M., and Langtry, R. 2003. "Ten years of industrial experience with the SST turbulence model." *Turbulence, Heat and Mass transfer* 4: 625-632.

Menter, F. R. 1994. "Two-equation eddy-viscosity turbulence models for engineering applications." *AIAA Journal* 32(8): 1598-1605.

Moghaddasi-Naini, H.R., Armfield, S. W., and Reizes, J. 1998. "Simulation of stratified flow around a square cylinder using the RNG k-epsilon turbulence model." *In: Proceedings of the 13th Australian Fluid Mechanics Conference*, Melbourne, Australia.

Muhm, J. M., Rock, P. B., McMullin, D. L., Jones, S. P., Lu, I. L., Eilers, K. D., Space, R. D., and McMullen, A. 2007. "Effect of aircraft-cabin altitude on passenger discomfort." *New England Journal of Medicine* 357(1): 18-27.

Müller, R. H. G., Scherer, T., Rötger, T., Schaumann, O., and Markwart, M. 1997. "Large body aircraft cabin a/c flow measurement by helium bubble tracking." *Journal of Flow Visualization and Image Processing* 4(3).

Olsen, S. J., Chang, H. L., Cheung, T. Y. Y., Tang, A. F. Y., Fisk, T. L., Ooi, S. P. L., Kuo, H. W., Jiang, D. D. S., Chen, K. T., Lando, J., Hsu, K. H., Chen, T. J., and Dowell, S. F. 2003. "Transmission of the severe acute respiratory syndrome on aircraft." *New England Journal of Medicine* 349(25): 2416-2422.

Olsson, M., and Fuchs, L. 1996. "Large eddy simulation of the proximal region of a spatially developing circular jet." *Physics of Fluids (1994-present)* 8(8): 2125-2137.

Orszag, S. A., Yakhot, V., Flannery, W. S., Boysan, F., Choudhury, D., Maruzewski, J., and Patel, B. 1993. "Renormalization group modeling and turbulence simulations." *Near-wall Turbulent Flows*: 1031-1046.

Patankar, S. 1980. *Numerical Heat Transfer and Fluid Flow*. Boca Raton, FL: CRC Press.

Peeters, T. W. J., and Henkes, R. A. W. M. 1992. "The Reynolds-stress model of turbulence applied to the natural-convection boundary layer along a heated vertical plate." *International Journal of Heat and Mass Transfer* 35(2): 403-420.

Pope, S. B. 2000. *Turbulent Flows*. Cambridge: Cambridge university press.

Pullen, J., Boris, J. P., Young, T., Patnaik, G., and Iselin, J. 2005. "A comparison of contaminant plume statistics from a Gaussian puff and urban CFD model for two large cities." *Atmospheric Environment* 39(6): 1049-1068.

Ricou, F. P., and Spalding, D. B. 1961. "Measurements of entrainment by axisymmetrical turbulent jets." *Journal of Fluid Mechanics* 11(01): 21-32.

Rohr, J. J., Itsweire, E. C., Helland, K. N., and Van Atta, C. W. 1988. Growth and decay of turbulence in a stably stratified shear flow. *Journal of Fluid Mechanics* 195: 77-111.

Russo, J. S., Dang, T. Q., and Khalifa, H. E. 2009. "Computational analysis of reduced-mixing personal ventilation jets." *Building and Environment* 44(8): 1559-1567.

Schumann, U., and Gerz, T. 1995. "Turbulent mixing in stably stratified shear flows." *Journal of Applied Meteorology* 34(1): 33-48.

Shi, Z., Chen, J., and Chen, Q. 2015. "On the turbulence models and turbulent Schmidt number in simulating stratified flows." Accepted by *Journal of Building Performance Simulation*.

Shih, T-H., Liou, W. W., Shabbir, A., Yang, Z., and Zhu, J. 1994. "A new k-epsilon eddy viscosity model for high Reynolds number turbulent flows: Model development and validation." *NASA STI/Recon Technical Report* N 95: 11442.

Smagorinsky, J. 1963. "General circulation experiments with the primitive equations: I. The basic experiment*." *Monthly Weather Review* 91(3): 99-164.

Sørensen, D. N., and Weschler, C. J. 2002. "Modeling-gas phase reactions in indoor environments using computational fluid dynamics." *Atmospheric Environment* 36 (1): 9-18.

Spall, R. E. 1998. "A numerical study of transient mixed convection in cylindrical thermal storage tanks." *International Journal of Heat and Mass Transfer* 41(13): 2003-2011.

Su, H. B., Shaw, R. H., Paw, K. T., Moeng, C. H., and Sullivan, P. P. 1998. "Turbulent statistics of neutrally stratified flow within and above a sparse forest from large-eddy simulation and field observations." *Boundary-Layer Meteorology* 88(3): 363-397.

Sze To, G. N., Wan, M. P., Chao, C. Y. H., Fang, L., and Melikov, A. 2009. "Experimental study of dispersion and deposition of expiratory aerosols in aircraft cabins and impact on infectious disease transmission." *Aerosol Science and Technology* 43(5): 466-485.

Tavoularis, S., and Corrsin, S. 1981. "Experiments in nearly homogenous turbulent shear flow with a uniform mean temperature gradient. Part 1." *Journal of Fluid Mechanics* 104: 311-347.

Tominaga, Y., and Stathopoulos, T. 2007. "Turbulent Schmidt numbers for CFD analysis with various types of flowfield." *Atmospheric Environment* 41(37): 8091-8099.

Umlauf, L., Burchard, H., and Hutter, K. 2003. "Extending the $k-\omega$ turbulence model towards oceanic applications." *Ocean Modelling* 5(3): 195-218.

Van Hooff, T., Blocken, B., Defraeye, T., Carmeliet, J., and Van Heijst, G. J. F.. 2012. "PIV measurements and analysis of transitional flow in a reduced-scale model: ventilation by a free plane jet with Coanda effect." *Building and Environment* 56: 301-313.

Venayagamoorthy, S. K., Koseff, J. R., Ferziger, J. H., and Shih, L. H. 2003. "Testing of RANS turbulence models for stratified flows based on DNS data. " Stanford: Stanford University environmental fluid mechanics laboratory.

Voke, P. R. 1996. "Subgrid-scale modelling at low mesh Reynolds number." *Theoretical and Computational Fluid Dynamics* 8(2): 131-143.

Wang, A., Zhang, Y., Sun, Y., and Wang, X. 2008. "Experimental study of ventilation effectiveness and air velocity distribution in an aircraft cabin mockup." *Building and Environment* 43(3): 337-343.

White, F. M., and Corfield, I. 2006. *Viscous Fluid Flow* 3. New York: McGraw-Hill.

Wilcox, D. C. 1988. "Multiscale model for turbulent flows." *AIAA Journal* 26(11): 1311-1320.

Wille, R., and Fernholz, H. 1965. "Report on the first European Mechanics Colloquium, on the Coanda effect." *Journal of Fluid Mechanics* 23(04): 801-819.

Wilcox, D. C. 1998. *Turbulence modeling for CFD*. Vol. 2. La Canada, CA: DCW industries.

Willmott, C. J., and Matsuura, K. 2005. "Advantages of the mean absolute error (MAE) over the root mean square error (RMSE) in assessing average model performance." *Climate Research* 30(1): 79.

Wu, C., and Ahmed, N. A. 2011. "Numerical Study of Transient Aircraft Cabin Flowfield with Unsteady Air Supply." *Journal of Aircraft* 48(6): 1994-2001.

Xu, D., and Chen, J. 2012. "Experimental study of stratified jet by simultaneous measurements of velocity and density fields." *Experiments in Fluids* 53(1): 145-162.

Yakhot, V., and Orszag, S. A. 1986. "Renormalization group analysis of turbulence. I. Basic theory." *Journal of Scientific Computing* 1(1): 3-51.

Yan, W., Zhang, Y., Sun, Y., and Li, D. 2009. "Experimental and CFD study of unsteady airborne pollutant transport within an aircraft cabin mock-up." *Building and Environment* 44(1): 34-43.

Yimer, I., Campbell, I., and Jiang, L. Y. 2002. "Estimation of the turbulent Schmidt number from experimental profiles of axial velocity and concentration for high-Reynolds-number jet flows." *Canadian Aeronautics and Space Journal* 48(3): 195-200.

Zhang, T., and Chen, Q. 2005. "Comparison of different ventilation systems for commercial aircraft cabins." *Proceedings of Indoor Air* 4: 3205-3210.

Zhang, T., and Chen, Q. Y. 2007. "Novel air distribution systems for commercial aircraft cabins." *Building and Environment* 42(4): 1675-1684.

Zhang, T. T., Yin, S., and Wang, S. 2010. "An under-aisle air distribution system facilitating humidification of commercial aircraft cabins." *Building and Environment* 45(4): 907-915.

Zhang, Y., Sun, Y., Wang, A., Topmiller, J. L., Bennett, J. S., and Besant, R. 2005. "Experimental characterization of airflows in aircraft cabins, Part II: Results and research recommendations. Discussion." *ASHRAE Transactions*: 53-59.

Zhang, Z., Chen, X., Mazumdar, S., Zhang, T., and Chen, Q. 2009. "Experimental and numerical investigation of airflow and contaminant transport in an airliner cabin mockup." *Building and Environment* 44(1): 85-94.

Zhou, X., Ouyang, Q., Lin, G., and Zhu, Y. 2006. "Impact of dynamic airflow on human thermal response." *Indoor Air* 16(5): 348-355.

LIST OF PUBLICATIONS

LIST OF PUBLICATIONS

Shi, Z., Chen, J., and Chen, Q. 2015. "On the turbulence models and turbulent Schmidt number in simulating stratified flows." Accepted by *Journal of Building Performance Simulation*.

Shi, Z., Chen, J., and Chen, Q. 2015. "Numerical simulation of Gasper-induced jet flow and its impact on air quality." Abstract submmited to *ISHVAC-COBEE* 2015.

Shi, Z., Chen, J., and Chen, Q. 2014. "Numerical study of flow characteristics and entrainment of stratified jet flows in enclosed environment." *Proceedings of the 13th International Conference on Air Distribution in Rooms (ROOMVENT 2014)*, pp. 622-629, Sao Paulo, Brazil.